# Accepted Manuscript

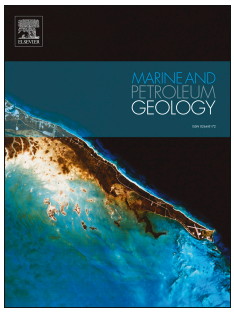


Monitoring land motion due to natural gas extraction: Validation of the intermittent SBAS (ISBAS) DInSAR algorithm over gas fields of North Holland, the Netherlands.

David Gee, Andrew Sowter, Alessandro Novellino, Stuart Marsh, Jon Gluyas

PII: S0264-8172(16)30269-0

DOI: 10.1016/j.marpetgeo.2016.08.014

Reference: JMPG 2650

To appear in: *Marine and Petroleum Geology*

Received Date: 6 May 2016

Revised Date: 9 August 2016

Accepted Date: 17 August 2016

Please cite this article as: Gee, D., Sowter, A., Novellino, A., Marsh, S., Gluyas, J., Monitoring land motion due to natural gas extraction: Validation of the intermittent SBAS (ISBAS) DInSAR algorithm over gas fields of North Holland, the Netherlands., *Marine and Petroleum Geology* (2016), doi: 10.1016/j.marpetgeo.2016.08.014.

# Monitoring land motion due to natural gas extraction: validation of the Intermittent SBAS (ISBAS) DInSAR algorithm over gas fields of North Holland, the Netherlands.

David Gee[a], Andrew Sowter[a*], Alessandro Novellino[b,] Stuart Marsh[a], Jon Gluyas[c]

[a]NGI, University of Nottingham, Nottingham NG7 2TU, UK.

[b]Geomatic Ventures Limited, Nottingham Geospatial Building, Nottingham NG7 2TU, UK.

[c]Department of Earth Sciences, Durham Energy Institute, Durham University, Durham, DH1 3LE, UK.

*Corresponding Author

*Keywords*

DInSAR, Intermittent SBAS, Gas production, Subsidence.

## Abstract

The differential interferometric synthetic aperture radar (DInSAR) remote sensing technique has proven to be invaluable in the remote monitoring of earth surface movements associated with the extraction and geostorage (subsurface injection) of natural resources (water, oil, gas). However, a significant limitation of this technique is the low density and uneven coverage that may be achieved over vegetated rural environments. The Intermittent Small Baseline Subset (ISBAS) method, an amended

version of the established SBAS algorithm, has been designed to improve coverage over rural, vegetated, land cover classes by allowing for the intermittent coherence that is predominant in such areas. In this paper we perform a validation of the ISBAS method over an area of gas production and geostorage in North Holland, the Netherlands. Forty-two ERS-2 (SAR) C-band images (1995-2000) and 63 ENVISAT (ASAR) C-band images (2003-2010) were processed using the ISBAS technique and the derived measurements enabled the identification of subsidence patterns in rural and urban areas alike. The dominant feature was an area of subsidence to the west of Alkmaar, attributed to natural gas production from the Bergermeer reservoir, where subsidence rates in the region of 3 mm/year were measured. Displacements derived using linear and non-linear surface deformation models were validated with respect to the first order system of levelling benchmarks which form the Amsterdam Ordnance Datum (NAP). It was established that ISBAS products were accurate to within 1.52 mm/year and 1.12 mm/year for the ERS and ENVISAT data sets respectively. Error budgets were comparable to results using persistent scatterers interferometry (PSI) during a validation activity carried out in the European Space Agency Terrafirma project. These results confirm the capability of the ISBAS method to provide a more regular sampling of land motion measurements over gas fields that may be critically used in future to infer the properties of buried, fluid-filled, porous rock.

## 1. Introduction

Satellite differential interferometric synthetic aperture radar (DInSAR) has proven itself to be an invaluable tool for monitoring land surface motion, capable of monitoring large areas at a low cost and at spatial scales not reasonably achievable by traditional in situ measurements (GPS surveys, slope inclinometers, tiltmeters, accelerometers, strain gauges and thermistors) and, sometimes, over areas not accessible at all (Milillo et al., 2015). Despite relatively few examples in the oil and gas industry (e.g., Ferretti, 2014), DInSAR is able to provide remarkable data, particularly for the upstream sector, namely the exploration, appraisal and production stages.

During exploration, SAR amplitude data can detect offshore oil slicks, e.g. oil seepages as an indicator of hydrocarbon existence (Leifer et al., 2012). During appraisal, ground motion results support site safety since risk areas of potential fault reactivation or possible well failure can be identified at an early stage (Davies et al., 2013; Wilson et al., 2015). During production DInSAR measurements can aid the assessment of whether the pressure of injection is correctly distributed over the area and the evaluation of the storage stability, since millimetric surface uplift could be one of the indicators for a potential storage leak. For Enhanced Oil Recovery operations, DInSAR monitoring is able to contribute to production efficiency (Yang et al., 2015). Finally, radar ground movement monitoring can be potentially used to provide warnings about potential risks for pipelines and Liquid Natural Gas terminals in areas suffering from landslides or subsidence hazard (Hole et al., 2012). The surface movement thus constitutes a signature

of the processes in the reservoir and can provide information about the surface and subsurface processes.

An early demonstration of this capability was on the In Salah Gas Project in Algeria from which gas production began in 2004 (Onumaa and Ohkawa, 2009; Ringrose et al., 2009). The produced natural gas from the individual fields within In Salah is not pure methane. Up to 10% $CO_2$ is present and this needs to be removed before the gas can be sold. BP and partners chose to re-inject the separated $CO_2$ rather than vent this greenhouse gas; storing it permanently underground in the same formations from which the natural gas is produced, albeit at a distance from the gas production areas (Bishop et al, 2004). As injection of $CO_2$ progressed, patterns of land surface heave were detected by DInSAR. Such data provided unique and critical information to the 4D reservoir model (spatial and temporal) that was invisible to conventional seismic surveys undertaken at the same time (Mathieson et al, 2009).

The In Salah project was undertaken in a non-vegetated, bare rock, desert area, which is excellent terrain for a DInSAR survey. This is because most DInSAR algorithms that span an extended period of time are limited to localities, typically rocky or urban terrain types, that unfailingly display high coherence or high phase stability for the entire period of image acquisitions. In the presence of vegetation, however, the majority of InSAR techniques either fail to work or provide very sparse coverage indeed (Crosetto et al., 2010; Osmanoğlu et al., 2015). Consequently, the spatial distribution of points is rarely sufficient to depict a large-scale feature that continues over dissimilar and dynamic land covers, such as may occur for an underground reservoir. As a result, only parts of the

subsidence patterns may be visible with some being missed altogether, which can lead to the incorrect interpretation of the results. This is a severe restriction to the application of DInSAR to reservoir monitoring in mid- and polar-latitudes as well as areas of tropical vegetation but not over desert areas, such as In Salah.

A potential solution to the vegetation problem is the Intermittent Small Baseline Subset (ISBAS) method (Sowter et al., 2013), developed at the University of Nottingham, which is a modification of the widely-used SBAS (Berardino et al., 2002) DInSAR time series processing algorithm. The modification recognises the intermittent nature of coherence over vegetated areas, exploiting this characteristic in an attempt to draw out the underlying land motion. Results have greatly increased the density of measurements over regions largely dominated by rural land cover, leading to a more consistent overall coverage and a more confident interpretation. It has been used to determine surface movements in various application areas including; coal extraction in the UK (Sowter et al., 2013, Novellino et al., 2014a, Bateson et al., 2015), landslips in Italy (Novellino et al., 2014b), elevation changes associated with blanket peat in Wales (Cigna et al., 2014) and groundwater abstraction in Mexico (Sowter et al., 2016).

There are a number of different ways to apply DInSAR to derive time series. Two broad categories exist (Hooper et al., 2012): ‘persistent scatterer’ and ‘small baseline’ approaches. Persistent scatterer approaches (e.g. Ferretti et al., 2001; Hooper et al., 2004; Kampes, 2005) target resolution pixels whose scattering characteristics remain constant when viewed from different angles and in time; whereas, small baseline approaches (e.g. Berardino et al., 2002; Mora et al., 2003; Schmidt and Bürgmann, 2003; Pepe et al., 2005; 2011; Lanari et al., 2007) target resolution cells that contain a distribution of

scatterers, inverting many interferograms to derive displacements. Additionally, there are algorithms that utilize both scattering types (e.g. Hooper, 2008; Ferretti et al., 2011). The ISBAS method is able to apply linear and non-linear models to land motion, to generate either a simple velocity per point or a profile of the deformation over time.

The ISBAS algorithm has previously been validated by contextual comparisons only, where the pattern of ground motion correlates with the geology and, in some cases, appears bound by existing fault structures (Bateson et al., 2015). This has essentially been motivated by the lack of historical survey observations in the vegetated classes. However, whilst a contextual interpretation provides spatial confirmation, there is a need for a more quantitative validation of ISBAS products. A geological validation cannot corroborate the rates of ground motion observed and there remains an amount of ambiguity and uncertainty around the algorithm's performance. Comparisons with existing surveyed observations on the ground can overcome this but, when using historical satellite observations as in this paper, there is seldom any off-the-shelf archive of ground truth with the desired spatial coverage or precision that were acquired with sufficient frequency during the specific period of the satellite observations. Furthermore, there is seldom any such data in rural locations where such measurements may be more difficult to procure.

Therefore, the principal aim of this paper is to conduct a quantitative validation of the ISBAS method through comparison with ground observations. In this aspect, we found an existing project was able to provide the necessary ground truth to achieve this: the Terrafirma Validation Project (TVP) (Crosetto et al., 2008; Hanssen et al., 2008). During this project, DInSAR surveys using persistent scatterers interferometry (PSI) were used to

monitor land movement in a gas production area in the Netherlands. The TVP ran within Stage 2 of the European Space Agency-funded Terrafirma project, demonstrating a significant PSI validation exercise of four Operational Service Providers (OSPs). The principle objective of the TVP was to validate motion data products via a product validation workgroup which brought together national geodetic and geological organisations, commercial radar remote sensing companies, government research institutions and end users to determine the consistency and accuracy of PSI motion monitoring. The TVP validation data set has been made publicly available specifically for the assessment of similar DInSAR algorithms. The availability of this data set therefore affords an opportunity to determine the accuracy of ISBAS products and to compare the accuracy of ISBAS with the PSI products generated by the TVP (Crosetto et al., 2008; Hanssen et al., 2008).

The main objective of this paper, then, is to apply the ISBAS DInSAR technique to SAR data of the gas fields of North Holland, validate the results using the TVP data and highlight any qualitative and quantitative improvements. We will conclude by underlining the implications of this for the future mapping and modelling of land surface displacements caused by gas fields. It should be noted this paper is focused on the validation of the ISBAS method, and is not a comparison against other processing algorithms designed to improve coverage in rural environments, such as SqueeSAR (Ferretti et al., 2011).

## 2. North Holland

### *2.1 Land Cover*

The area of interest (AOI) for the validation is situated in North Holland, the Netherlands, and covers an area of 517 square kilometres (fig. 1a). Five different basic land cover classes were determined using a supervised classification on a Landsat 7 Enhanced Thematic Mapper Plus (ETM+) image acquired on 24th August 2000.

The results of the classification are shown in fig. 1b. The land cover consists of: 69% agricultural fields, 0.1% sand dunes, 22.1% urban districts, 0.8% water bodies and 8.1% woodland. Mixed agriculture dominates in the province, with much of the best agricultural land found below sea level on reclaimed polders. The west coast is characterised by a long thin belt of sand dunes that protect the province from the North Sea. The AOI contains the cities of Alkmaar and Heerhugowaard; and the towns of Broek op Langedijk, Bergen, Heiloo, Castricum, Utigeest, Krommenie and Wormerveer.

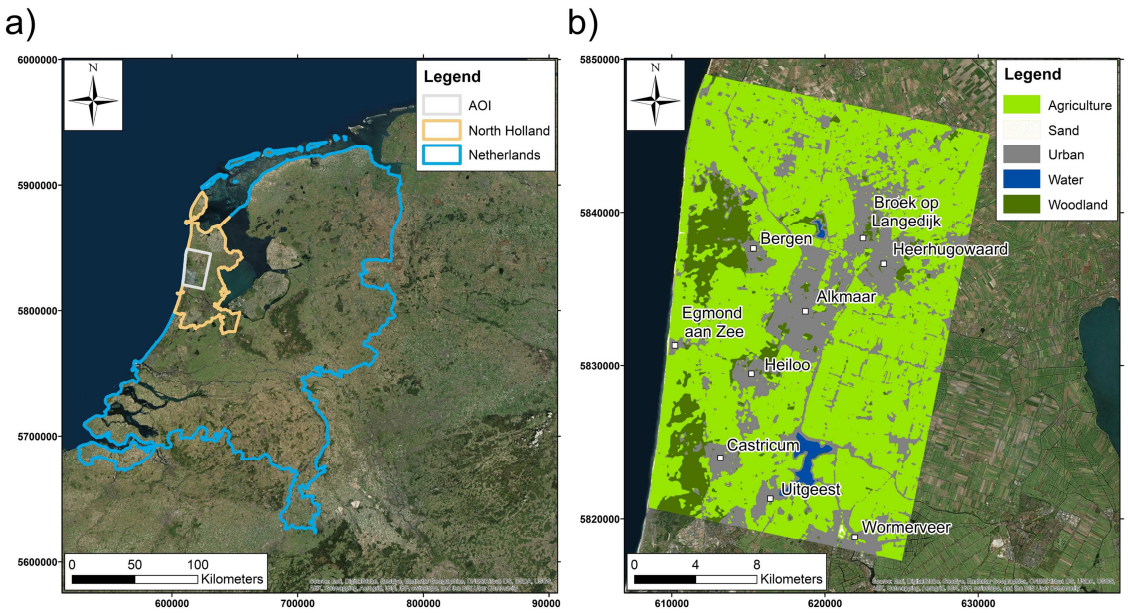

**Fig. 1**. (a) Map locating the North Holland province and area of interest (AOI) within the Netherlands (b) Land cover classification of the AOI conducted on Landsat 7 ETM+ imagery (24th August 2000).

*2.2 History of Gas Production*

After Groningen, the largest natural gas field in Europe, the Alkmaar area is the most important gas-producing region in the Netherlands (Grötsch and Gaupp, 2011). Exploration began in 1962 when the Amoco Netherlands Petroleum Company commenced drilling. The Amoco group discovered the Heiloo and Schermer reservoirs in 1964 (fig. 2); however, in November 1965 the Dutch government suspended drilling awaiting an enactment of exploration legislation, which arrived on May 3rd 1967 when the Mineral Exploration Act was published. Operations progressed slowly due to legislative issues and environmental protest groups. The surface environment of the area presents a challenge with respect to exploration and production; much of the northwestern part of the country is located below sea level, protected from the sea by sand dunes. The polder land and dunes have their own ecological balance which is predominantly controlled by ground-water conditions. The ecological and economic quality of the polder land below sea level is maintained by strict management of surface and ground water. The dunes constitute a vast fresh-water reservoir, utilized as a drinking water reserve, and is therefore protected against any activity that might jeopardize its integrity such as drilling operations or seismic activity. Additionally, the area contains a nature reserve and the historic city of Alkmaar. Any disruption the flora and fauna of the reserve and the century old buildings of Alkmaar would have been unacceptable and

therefore it was not until September 1972 that the first field, Bergermeer, came on stream. It was swiftly followed by Groet in 1974, Bergen in 1978, Schermer and Alkmaar in 1979 and Heiloo in 1982 (Van Lith, 1983). The locations of these fields are shown in fig. 2.

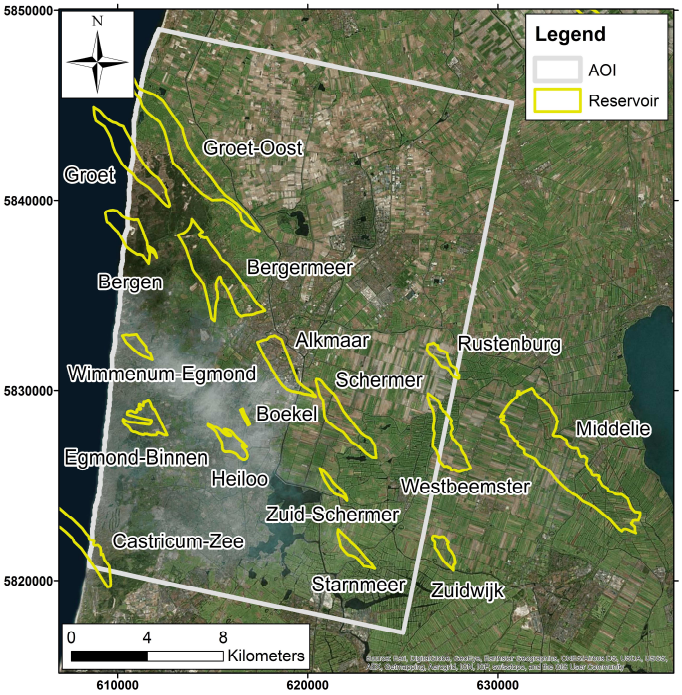


**Fig. 2.** Location map showing the AOI and the gas fields

*2.3 Geological Setting*

Productive reservoirs have been found at depth from 1200 to 2000 m in the Permian, Upper Rotliegend Group, Zechstein Group and Lower German Triassic Group (Buntsandstein) (Kaasschieter and Reijers, 1982). In the Alkmaar area all formations consist of sedimentary rocks; the oldest formations drilled belong to the Limburg Group (Late Carboniferous) which is unconformably (Saalian unconformity) overlain by the Early Permian Upper Rotliegend Group, the main gas reservoir (fig. 3). The Upper Rotliegend group encompasses coarse (e.g., Slochteren Formation) and fine-grained (e.g., Silverpit Formation) clastic sediments, predominantly of red-bed type, as well as

evaporites with a thickness in the order of 200 to 270 m (Van Adrichem Boogaert, 1976). The net-to-gross ratio is quite high (>80%) in the moderately cemented sandstone layers with porosity in the 15-20% range. The lower boundary of the Zechstein Group in the basin has been taken at the base of the Coppershale, a thin, black, bituminous shale bed recognized over practically the entire Southern Permian Basin, which provides an excellent marker horizon (fig. 3). In addition, a series of subsequent evaporite layers, due to a marine transgression, function as a sealing layer of the Rotliegend Group reservoir rock.

The Zechstein Group accumulated as a series of marine/playa sequences consisting of anhydrite, carbonate and clay for a total thickness of ≈200 m in the study area (Van Gent et al., 2011) where another reservoir, the Z3 Leine Formation (Plattendolomite), occurs. The Z3 Leine Formation is a light brown dolomite with intercrystalline and locally vuggy porosity, interbedded with light to dark grey, argillaceous and slightly carbonaceous, dense dolomite, with a thickness of 40-50 m. The Plattendolomite reservoir has a variable quality with porespace changing from a few percent to 20%; much of its porosity is vuggy or intercrystalline and interconnected via pervasive fractures and joints. As for the Zechstein Group, the Buntsandstein name has also been derived from the German stratigraphic nomenclature of the Triassic period. The Buntsandstein is a group of formations composed mainly of ≈300 m red-bed-type sandstones, siltstones and claystones, situated between the top of the Zechstein Group and the Base Solling Unconformity (also known as Spathian Unconformity), which marks the base of the Upper Germanic Trias Group. Differently, the base is characterized by a succession of

red-brown to green silty, sometimes anhydritic claystones (the Main Claystone Member) which overlay the Zechstein strata (fig. 3). The net-to-gross ratio in the Buntsandstein is as high as is the porosity, typically 20-25%.

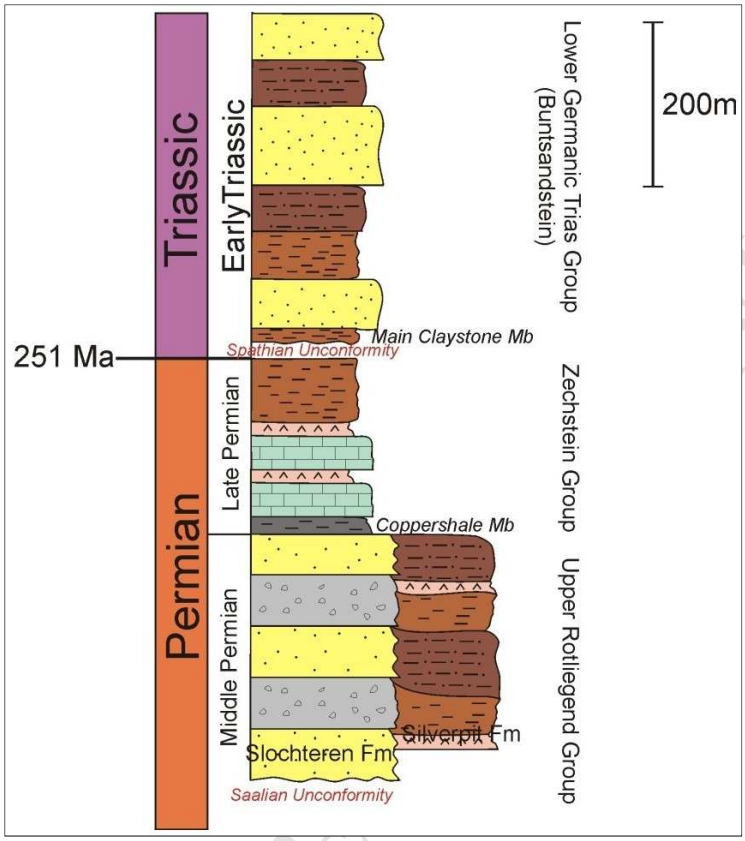


**Fig. 3.** Schematic stratigraphy of the study area for the Middle Permian Epoch to Early Triassic Epoch. Fm=Formation; Mb=Member.

*2.4 Reservoir Compaction and Induced Seismicity*

Vertical land movements, the variation in the position of land with respect to sea-level, have been inferred to occur in the Netherlands using different geodetic and geological indicators (Kooi and De Vries, 1998). Contributions to this changing land–sea relationship include different and, overlapping, geological processes: the long-term tectonic and isostatic subsidence of the crust, representative for time scales of 106-107yr, and others at shorter time scales of 100-103 yr, such as the Pleistocene sands (Kooi and De Vries, 1998) and reservoir compaction related to gas production (Lorentz et al., 1995), which in the AOI, is the predominant phenomenon, and is often associated with induced seismicity (van Wees et al., 2014).

The compaction of a porous medium, such as reservoir layers and acquifers, relates to the Terzaghi's principle of one-dimensional consolidation (Terzaghi, 1925). Under this principle, when the total stress remains constant, a change in pore fluid pressure causes an equivalent change in the effective stress within the reservoir system, which causes the system skeleton to compress or expand under the new load. Therefore, if effective stress is increased by fluid withdrawn, the reservoir system compresses elastically. The degree of resulting compaction depends on the compressibility of the reservoir rock, reservoir thickness and its depositional history and boundary conditions (Gluyas and Cade, 1997; Galloway et al., 1998; Nagel, 2001).

Continually, the poroelastic theory, formulated by Geertsma (1957; 1966), has specifically addressed the rock mechanical problem of reservoir compaction due to production pressure depletion through the stress–strain relationship.

The consequences of the subsurface compaction affect both hydrocarbon production and reservoir management, arising safety issues related to platform stability and environmental impact.

Seismic events are a further consequence of gas production and are often associated with reservoir compaction (Wilson et al., 2015). They occur as a result of slip on pre-existing surfaces (Zoback and Zinke, 2002), which can be initiated by a variety of mechanisms including geochemical reactions, pore pressure variations, temperature effects and the reactivation or locking of pre-existing faults (Suckale, 2009). Induced seismic activity in the north of the Netherlands began in 1986; five notable events have previously occurred in the area of interest, four in the Bergermeer reservoir and one the Bergen reservoir (Haak et al., 2001). Despite small earthquakes ≤3.5ML, the Alkmaar area is considered an area of low seismic hazard (van Eck et al., 2006), constituting less of a risk than the Groningen gas field in north-eastern Netherlands (TNO, 2015; van Thienen-Visser and Breunese, 2015). Dutch mining legislation introduced in 2003 requires that operators assess seismic hazard as part of a risk appraisal before exploration and production licenses can be awarded (van Eijs et al., 2006).

## 3. ISBAS Analysis

### *3.1 Processing*

Forty-two ERS-2 SAR descending images acquired between 19th July 1995 and 16th August 2000 (Table A.1) and sixty-three ENVISAT ASAR descending images acquired between 19th March 2003 and 8th September 2010 (Table A.2) were processed separately using the ISBAS technique. Both data sets had restrictions of a maximum of 250m on the perpendicular baseline and four years on the temporal baseline applied, values commonly applied to SBAS surveys. Multilooking (spatial averaging of pixels) was implemented using a 4 x 20 window size, producing pixels of 100m x 100m in ground range and points deemed coherent were those which displayed an average coherence greater or equal to 0.25, a threshold again common to SBAS surveys using ERS or ENVISAT data.

The perpendicular orbital baseline (Bperp) relative to the master, plotted against the relative time (temporal baseline) of each image is illustrated for each case in fig.4. Each image appears as a vertex and, when a pair of images forms a differential interferogram meeting the restrictions, a line is drawn between them, as illustrated.

ISBAS processing is then performed only on points that meet a minimum quality criterion (called coherent points). This criterion is based upon that point being of sufficient quality in a minimum number of interferograms. If there are $N$ interferograms in total, an interferogram threshold $m$ (such that $m \leq N$) is selected such that, if the point shows sufficient quality (coherence) in a minimum of $m$ interferograms then it is used; otherwise, it is discarded. This rule allows the ISBAS algorithm to accept points that may not be high quality in all interferograms, which is a characteristic of vegetated sites.

It must be recognised that points with a high value of *m* are high quality, meaning that they are more coherent. However, such points are fewer and would likely not provide sufficient coverage of all land cover classes. The choice of *m*, therefore, is a trade-off between coverage and quality. The values of *m* have a direct relationship to the final standard error (Cigna et al., 2014) and so a good value based on coverage and acceptable standard error can be estimated on a case-by-case basis.

In all aspects of the processing, close attention was made to the quality of intermediate stages, such as phase unwrapping, and identifying the presence of any anomalous effects such as persistent atmospheric anomalies. No obvious errors were detected or were filtered out during baseline correction.

The ERS data analysis resulted in 294 multi-looked differential interferograms (fig.4a) and an interferogram threshold of $m = 90$ was applied. The derivation of linear velocities for each coherent point was then performed using a reference point at 52°38'02.7"N 4°45'56.2"E located in Alkmaar. Reference points act as a benchmark for the deformation (i.e. all derived deformations are relative to this point). For this reason, these points are expected to be stable, of zero velocity, and, to aid the analysis, highly coherent in all *N* interferograms. To ensure the ground motion was relative to a stable location, the reference points were located in areas where levelling data indicated it was most stable during the period of observation, which was different for the ERS and ENVISAT data analysis.

The ENVISAT data analysis resulted in 636 multi-looked differential interferograms (fig. 4b) and an interferogram threshold of $m = 210$ was used. The derivation of linear

velocities used a reference point at 52°35'47.2"N 4°42'33.2"E, located in the town of Heiloo, approximately 2km south west of Alkmaar.

The analysis results in a line-of-sight (LOS) velocity ($v_{LOS}$) for each coherent point, towards or away from the satellite. If we simplistically assume that all motion is vertical, to enable an equivalent comparison with the results of the TVP, the vertical velocity ($v_{vert}$) is given by:

$$v_{vert} = \frac{v_{LOS}}{cos\theta} \quad (2)$$

where $\theta$ is the incidence angle from the surface normal, approximately 23° at scene centre for both of the ERS and ENVISAT frames used here.

One of the benefits of the ISBAS analysis is that the increased density of points processed allows phase unwrapping to be performed in confidence across the entire area of the image. Here, the ISBAS analysis was actually performed on the complete 100 km x 100 km image frame in both ERS and ENVISAT cases.

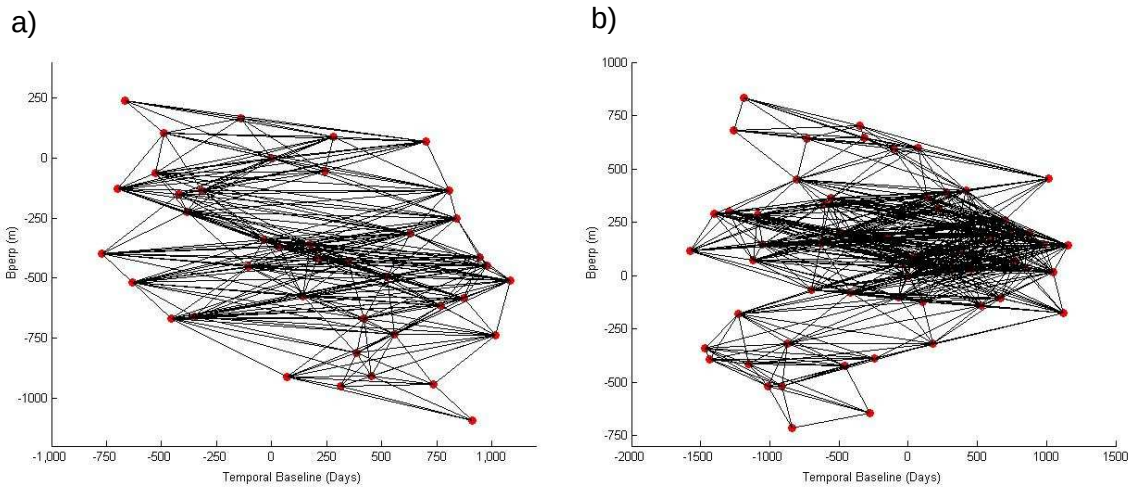


**Fig. 4.** Temporal and perpendicular baselines of the image pairs relative to the master (a) ERS SAR (master: 27th August 1997) (b) ENVISAT ASAR (master: 11th July 2007).

*3.2 Results using a Linear Model of Deformation*

Using a linear model of the deformation results in the generation of rates of motion (velocities) for each coherent point across the scene. These are shown in fig. 5.

In the ERS case, coherent points covered 80% of the total land surface contained in the entire frame (fig. 5a). The distribution of point velocities was densest in urban regions but also extended into rural areas, over agricultural fields and woodland. The complete image frame contains several areas of deformation that fall outside of the AOI and are not the subject of this paper. However, it is interesting to note that the largest area of deformation, in the southwest of the frame, appears to correspond to a peatland area known as the Green Heart (Groene Hart), already the subject of DInSAR surveys (Cuenca and Hanssen, 2008) and also falling in a predominantly rural region.

In the ENVISAT case, coherent points covered 88% of the total land area of the full frame (fig. 5b). Following the same trend of the ERS analysis, the ISBAS result produced a wide and even spread of point velocities across the scene. However, as will be discussed below, the amount of deformation observed was far less than in the ERS survey.

As indicated above, the best quality points occur when $m=N$ (i.e. $m$=294 for ERS and $m$=636 for ENVISAT). However, these points account for only 7% of the ERS and 10% of the ENVISAT total land cover. Furthermore, the distribution of these points are limited to urban centers and other locations where scatterers are more stable and decorrelation is less prominent. For instance, considering only the ERS points that lie within the area of interest (AOI), 74% of such points are located in urban land cover (and urban land cover only makes up 22% of AOI).

Below we will discuss the linear deformation results within the AOI boundary for the ERS and ENVISAT surveys, respectively.

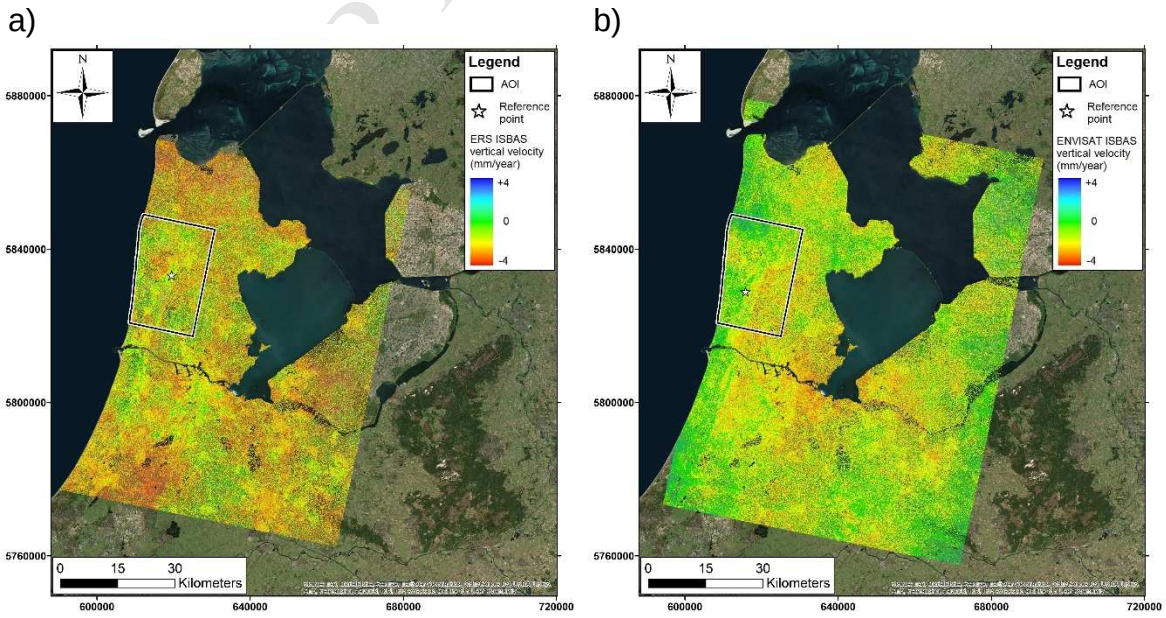

**Fig. 5.** (a) ERS ISBAS vertical velocities (b) ENVISAT ISBAS vertical velocities.

*ERS*

In the AOI the mean velocity of all points was -0.93 ± 1.09 mm/year with a maximum subsidence of -7.45 ± 1.59 mm/year and a maximum uplift of 4.55 ± 1.17 mm/year (fig. 6a); the standard error ranged from 0.27 – 2.29 mm/year (fig. 6c). Lower standard errors are observed in urban areas, as may be expected due to the likelihood of more coherent interferograms per point, *m* (fig. 6e). The predominant source of error is seen within targets exhibiting intermittent coherence, with a strong correlation in relation to the standard error and the number of interferograms used in the calculation of the velocity (fig. 6c and fig.6e).

Overall, the AOI displays little ground motion and where motion does occur it is relatively small, up to around 3mm/year maximum (fig. 6a). The most significant area of ground motion is located to the west of Alkmaar, where a clear boundary of stability and subsidence can be seen at the edge of urban Alkmaar. Ground motion here can be attributed to natural gas extraction as the results show good correlation with the extents of the Bergermeer reservoir (fig. 6a and fig.9c). Although the deformation is large enough to be detected, the pattern appears noisy, particularly in the rural areas where there is a higher standard error (Table 3). Our confidence in identifying this signal as real deformation depends on its relative strength to the background noise and, in this case, a rate of 3mm/year is just above the 99% confidence level (3 sigma). Had a greater level of

deformation signal been present in the data a smoother more confident subsidence pattern would almost certainly have been observed, as was present in previous studies of spatially correlated motion using the technique (Bateson et al., 2015; Sowter et al., 2013; Sowter et al., 2016).

*ENVISAT*

Following the ISBAS analysis the mean velocity of all points in the AOI was -0.33 ± 0.65 mm/year, with a maximum deformation of -3.91 ± 0.86 mm/year and maximum uplift of 3.64 ± 0.74 mm/year (fig. 6b). The ISBAS standard error ranged from 0.17 – 1.12 mm/year (fig. 6d). Similarly to the ERS results, higher standard deviations were seen in rural areas due to the reduced likelihood of coherent interferograms per point, *m* (fig. 6d and fig. 6f). The same correlation is found with regards to the standard error and *m*, confirming that the main source of error is found in points encompassing intermittent coherence, predominantly located rural areas (Table 3).

There was a much smaller deformation signal in the ENVISAT data, which proved to be more stable than the ERS survey (fig. 6a and fig. 6b). There is still a very minor pattern that follows the trend with the ERS time series where points over Alkmaar are stable and with some subsidence to the northwest in the region of the Bergermeer reservoir and southeast in the region of the Schermer reservoir (fig. 6b).

| | ***Agriculture*** | ***Sand*** | ***Urban*** | ***Woodland*** |
|---|---|---|---|---|
| **ERS standard error (mm/year)** | | | | |
| Mean | 1.17 | 1.14 | 0.84 | 1.19 |
| Range | 0.34-2.29 | 0.61-1.54 | 0.27-2.04 | 0.37-1.94 |

| | | | | |
|---|---|---|---|---|
| **ENVISAT stand error (mm/year)** | | | | |
| Mean | 0.70 | 0.56 | 0.50 | 0.66 |
| Range | 0.25-1.12 | 0.40-0.92 | 0.17-1.03 | 0.26-0.94 |

**Table 3**

Standard error per land cover classification within the area of interest (AOI).

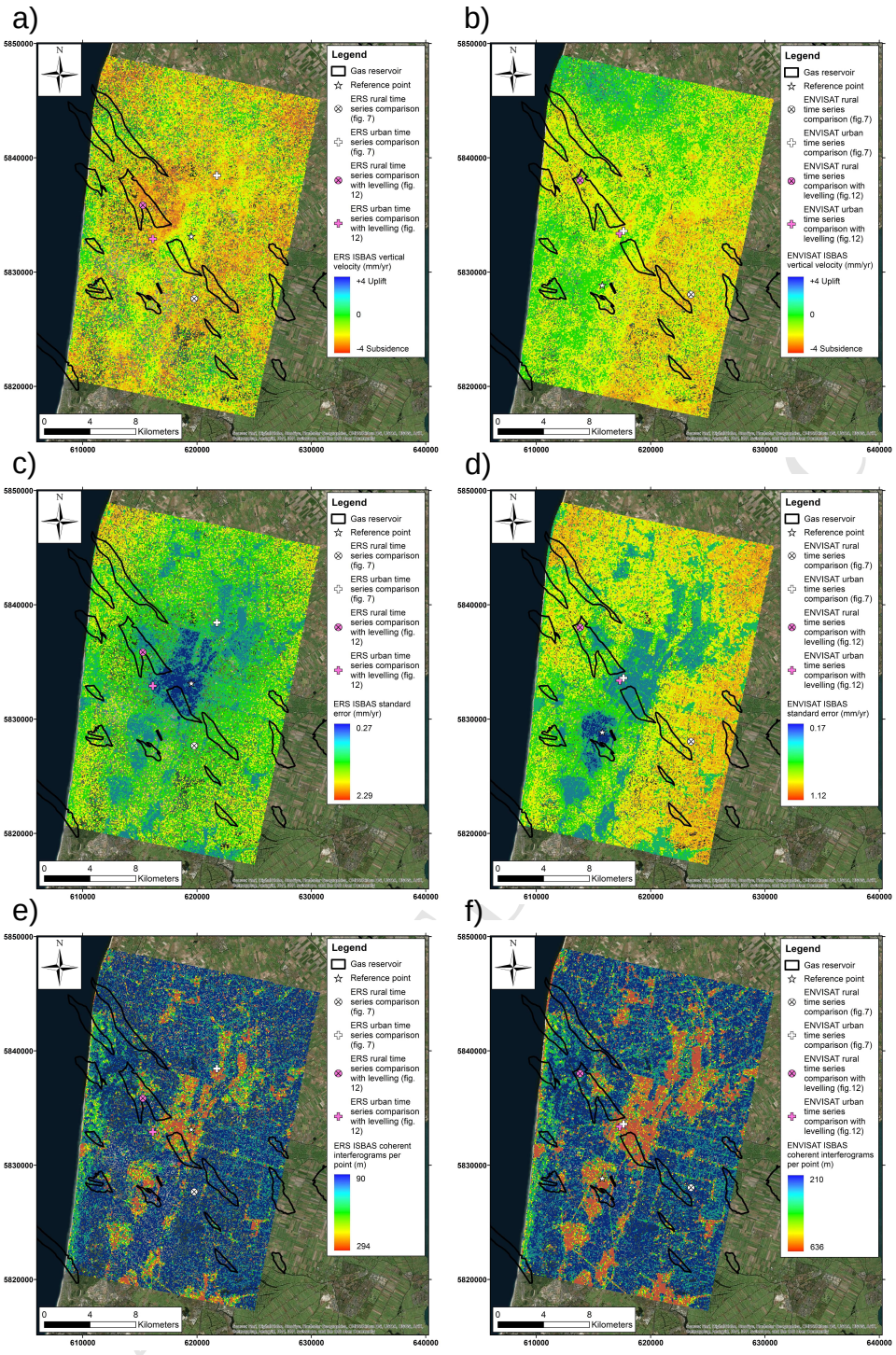


**Fig. 6.** (a) ERS ISBAS vertical velocities (b) ENVISAT ISBAS vertical velocities (c) ERS ISBAS standard error (d) ENVISAT ISBAS standard error. (e) ERS ISBAS

coherent interferograms per point (*m*) (f) ENVISAT ISBAS coherent interferograms per point (*m*).

*3.3 Results using a Non-Linear Model of Deformation*

A non-linear model was applied to both ERS and ENVISAT datasets, using a similar method as that proposed by Berardino et al. (2002) for SBAS. This method systematically applies temporal and spatial filters to deduce the atmospheric phase screen from the phase residuals and the accuracy is difficult to determine without comparison against detailed profiles. Ground truth for InSAR measurements are rarely available in sufficient densities, to within the desired precision and are often unreliable, difficulties which are more restrictive to validation attempts in rural environments. It is notoriously difficult to implement quality control due to the absence of a known scatterer, the phase ambiguity estimation problem and the absence of redundant measurements (Marinkovic et al., 2007).

Fig. 7 displays the resulting deformation time series of four arbitrarily selected coherent points, the locations of which are marked on fig. 6. In these examples two points were selected from urban and rural land covers for both ERS and ENVISAT data sets, respectively. It is evident that ISBAS points that fall in agricultural or woodland areas (fig. 7b and fig. 7d) are noisy when compared with the results of the linear displacement model; ISBAS points that fall in urban areas (fig. 7a and fig. 7c) are far less noisy and follow closely the linear model. This is reflected in the standard errors, which are greater for points falling in rural areas because of the reduction in the quantity of coherent interferograms per point (*m*) and potentially the network used for the inversion. The

standard error is over twice as high over vegetation in both the ERS and ENVISAT data sets which may also be used as an indication of the unreliability of time series outside of urban classes.

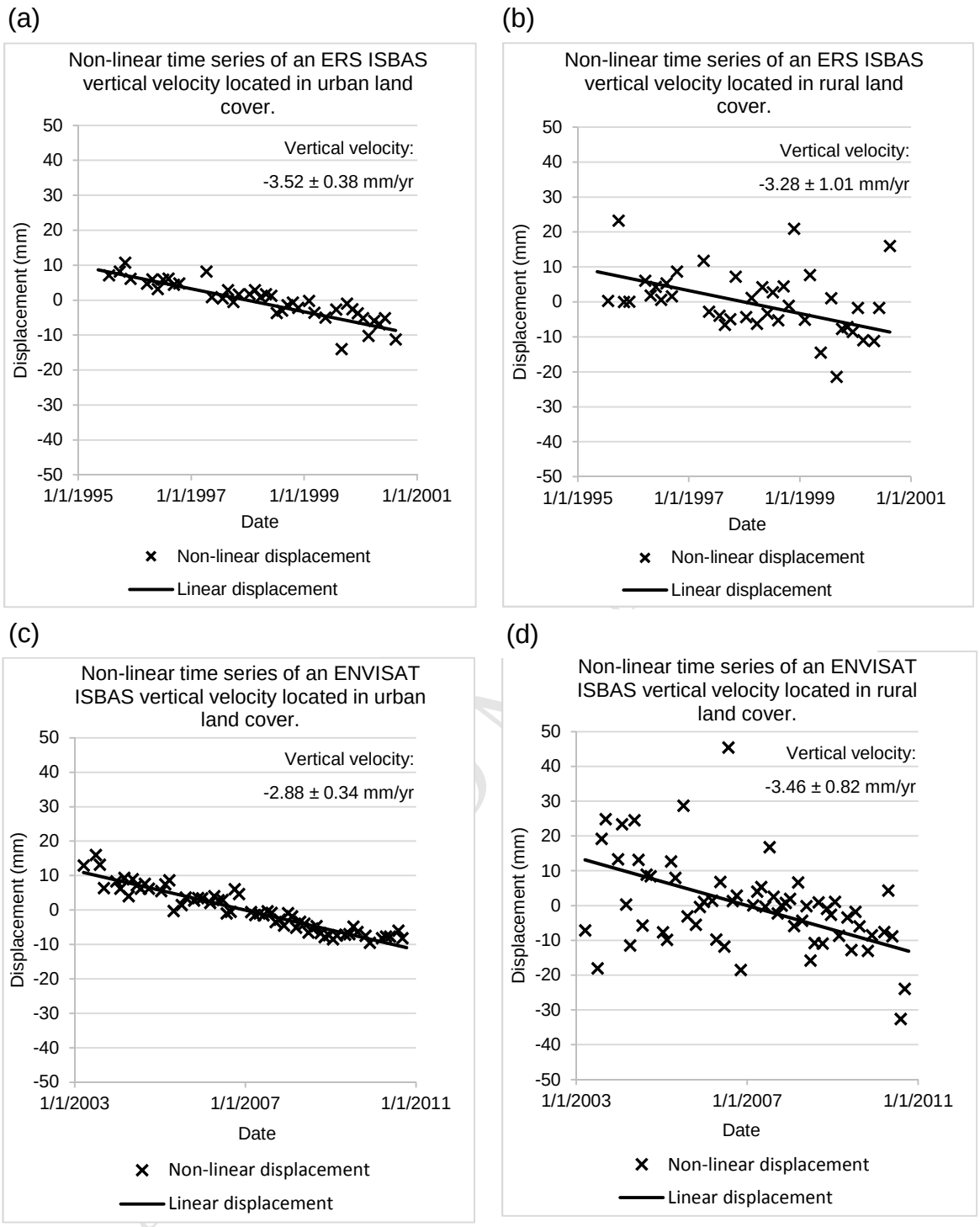


**Fig. 7.** Non-linear time series for selected ISBAS points. The crosses represent the ISBAS non-linear displacements and the lines represents the ISBAS linear displacements which were derived separately. (a) ERS ISBAS in urban land cover (b) ERS ISBAS in

rural land cover (c) ENVISAT ISBAS in urban land cover (d) ENVISAT ISBAS in rural land cover.

## 4. Results

### *4.1 Levelling Benchmarks*

Levelling data were provided to the TVP by the Rijkswaterstaat. Benchmarks attained were of the 1st order which define the Amsterdam Ordnance Datum (NAP), located approximately 30 metres below the surface established on Pleistocene sand deposits. Benchmarks for the ERS and ENVISAT validation were prepared separately, with levelling campaigns approximately four years before and after the radar acquisitions being utilized. There were five significant campaigns that contained over 200 measurements in the ERS validation and four campaigns with over 200 measurements in the ENVISAT validation. Estimates of displacement velocities from the levelling data were computed for each benchmark, fitting a linear trend through the levelling heights. Only those benchmarks that had three or more measurements were used in the validation to ensure confidence in the calculated velocity. Fig. 8 displays an example of a levelling benchmark used in the ERS validation, where it is evident that a linear model is suitable for the observed subsidence. Once fitted, linear velocities could be calculated; 235 benchmarks satisfied the conditions for the ERS validation and 210 for the ENVISAT validation. The quality of the heights estimated from levelling benchmarks can only be estimated, as precise information is not available. The original levelling data has a precision of 0.7 mm per square kilometer, but the variance-covariance matrix of the heights could not be reconstructed due to unknown network design and adjustment

procedures. Consequently, as was assumed in the TVP, the heights are presumed to be uncorrelated with a standard deviation of 1 mm/year.

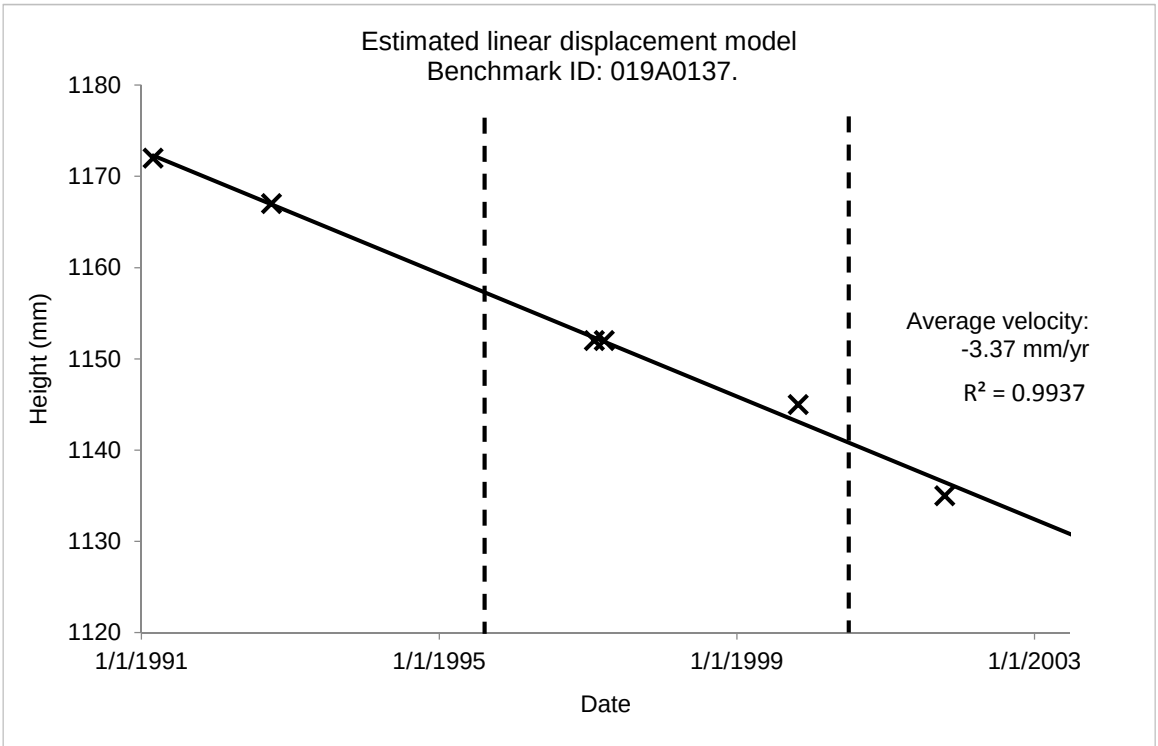


**Fig. 8.** The linear displacement model estimated for Benchmark ID:019A0137 for the ERS time series. The vertical dashed lines represent the start and end of the SAR acquisitions.

*4.2 The Spatial Distribution of the Linear Deformation Results*

To qualitatively investigate the spatial relationship between the ISBAS-derived linear velocities and the velocity of the levelling benchmarks, levelling benchmarks were overlaid on ISBAS products. The results are in approximate agreement; it is evident that in the ERS data both the ISBAS and levelling techniques have identified an area of

subsidence around the Bergermeer reservoir, while there is a lack of motion over the city of Alkmaar (fig. 9a and fig. 9c). The ENVISAT data shows a similar pattern but the subsidence rates over the Bergermeer reservoir have fallen considerably, whereas Alkmaar remains stable (fig. 9b and fig. 9d). Crucially, there is a consistency between the data; both in the patterns of stability and subsidence identified by the levelling and ISBAS analysis and in the differences between the ERS and ENVISAT data, where higher rates of subsidence area identified in the ERS data. In addition, the assumed accuracy of the levelling heights is ±1mm/year, while within the AOI the mean standard error of ISBAS points in the ERS analysis was 1.00 mm/year. Consequently, on average up to a 2 mm/year difference between velocities derived from ISBAS analysis and levelling could be accounted for in the standard errors.

The ISBAS analysis appears to give excellent coverage over the complete site; with coverage achieved in rural land cover at locations over the gas reservoirs. The ISBAS analysis covers most of the region extending over woodland and agricultural areas and demonstrates that subsidence occurs across this region. Points are certainly less reliable in rural areas but we can still be measurably confident about such points as demonstrated by the standard error. Despite the intermittent nature of coherent ISBAS targets, the coverage has not come at the sacrifice of the quality with a mean standard error in the AOI of 1.00 mm/year and 0.65 mm/year for the ERS and ENVISAT data sets respectively. If warranted by the quantitative analysis, the additional coverage would clearly be of benefit as it provides a more complete description of the spatial distribution of deformation.

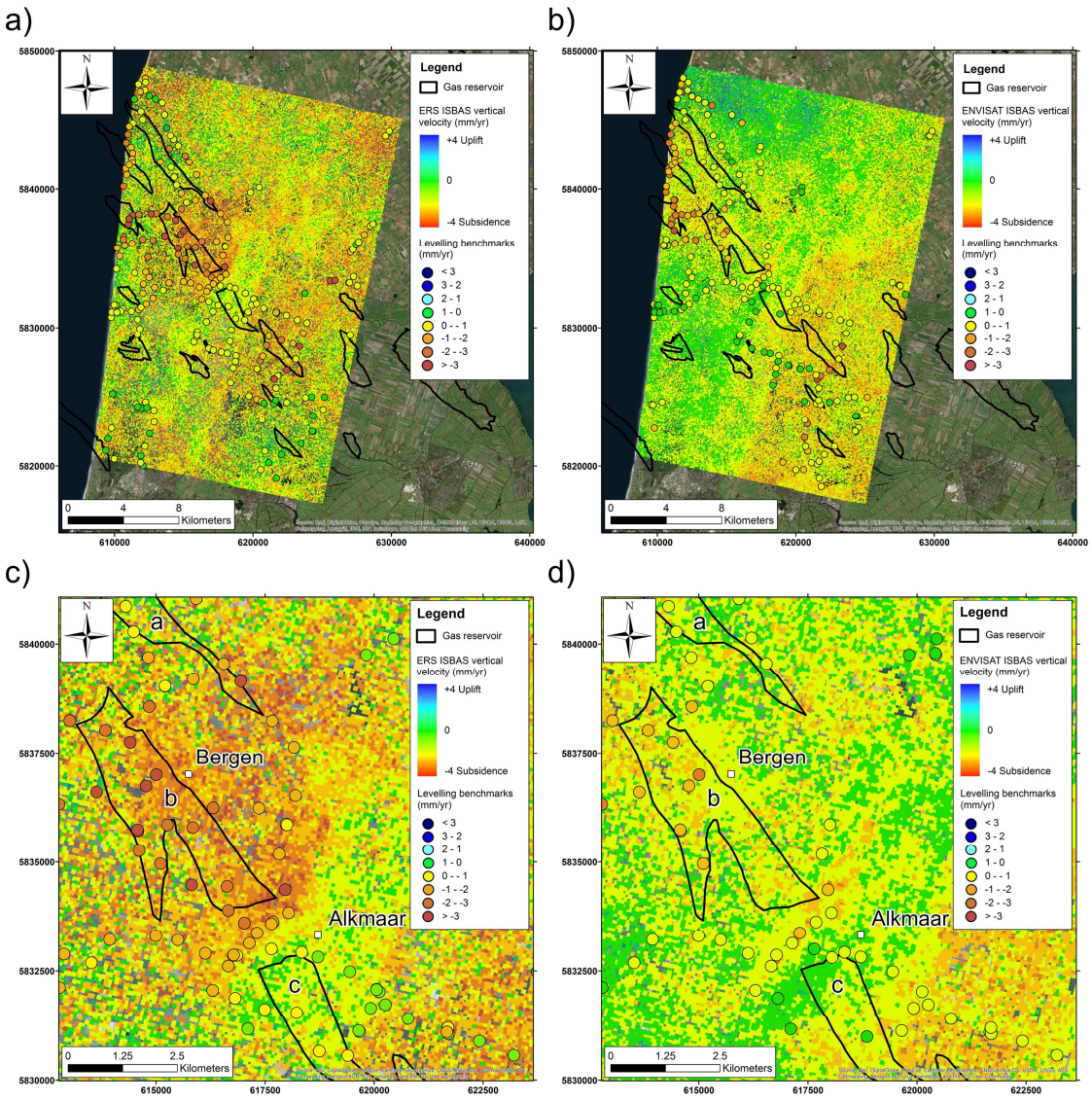


**Fig. 9.** (a) ERS ISBAS vertical velocities with levelling benchmarks overlaid (b) ENVISAT ISBAS vertical velocities with levelling benchmarks overlaid. (c) ERS ISBAS vertical velocities with levelling benchmarks overlaid in the area of Alkmaar (d) ENVISAT ISBAS vertical velocities with levelling benchmarks overlaid in the area of Alkmaar. a marks the Groet-Oost reservoir, b the Bergermeer reservoir and c the Alkmaar reservoir.

*4.3 Quantitative Comparison of the Measured Linear Velocities*

In this analysis, ISBAS point velocities are directly compared with the levelling measurements. However, it is important to recognise that the ISBAS velocities correspond to an area of approximately 100m x 100m whereas the levelling points are likely made on isolated survey pegs or nails corresponding to dimensions of only a few centimetres at most. On the assumption that the velocity of the levelling point was characteristic of its surroundings, each levelling benchmark velocity was compared with the nearest point velocity from the ISBAS survey and, where no ISBAS velocity fell within 50 metres, the levelling benchmark was discarded from the analysis. This left each remaining levelling benchmark with a corresponding ISBAS point velocity for comparison.

One hundred and twenty-eight levelling benchmarks fulfilled the criteria for the ERS ISBAS/levelling validation and 187 locations for the ENVISAT ISBAS/levelling validation. The root mean square error (RMSE) of the difference between the two measurements for the ERS velocities was 1.52 mm/year while the ENVISAT case produced a smaller RMSE of 1.13 mm/year (Table 4). The histograms of the differences are displayed in fig. 10.

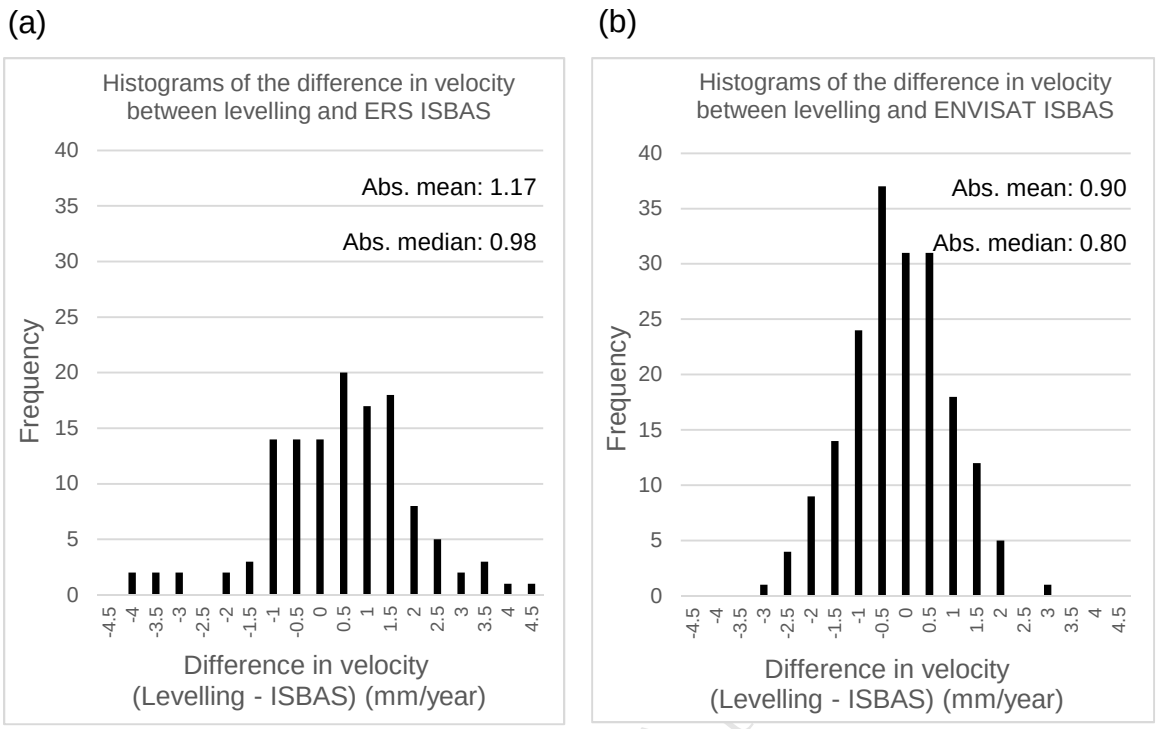


**Fig. 10.** Histograms of the difference in velocity (Levelling velocity – ISBAS velocity) (a) ERS (b) ENVISAT. Abs=Absolute.

As previously stated, the predominant source of error is seen within targets exhibiting intermittent coherence (rural areas), with a correlation between the standard error and *m* (fig. 6). It was therefore investigated whether the high quality points, predominantly found in urban areas, produced a smaller error with respect to levelling. The ISBAS analysis was divided into two categories, rural and urban. The RMSE was calculated for urban points and for rural points. A large difference was found in the ERS data where points with constant coherence were 0.47 mm/year more accurate than those displaying intermittent coherence. The difference was far smaller in the ENVISAT data where

points with constant coherence only 0.06 mm/year more accurate than those displaying intermittent coherence. Table 4 summarizes the results.

Previous investigations have shown that other DInSAR techniques are limited in their spatial coverage, typically restricted to urban and rocky environments (e.g., Li et al., 2014; Osmanoglu et al., 2015; Gong et al., 2016). Prior studies using the ISBAS method have demonstrated that the spatial extent of ISBAS velocities is improved and the patterns of land motion correlate to geology (Sowter et al., 2013; Bateson et al., 2015). Here, we have shown a similar improvement in spatial coverage and also report that, where available, the quantitative measurements are correct.

| | ***ISBAS*** | ***Urban ISBAS*** | ***Rural ISBAS*** |
|---|---|---|---|
| **ERS** | | | |
| No. of Benchmarks | 128 | 24 | 104 |
| RMSE ISBAS-Levelling (mm/year) | 1.52 | 1.05 | 1.61 |
| **ENVISAT** | | | |
| No. of Benchmarks | 187 | 26 | 161 |
| RMSE ISBAS- Levelling (mm/year) | 1.13 | 1.07 | 1.14 |

**Table 4**

RMSE between ISBAS-levelling.

*4.4 Comparison of Non-Linear Time Series and Levelling*

Fig. 11 displays a comparison of the displacements derived from the linear ISBAS analysis, the non-linear ISBAS analysis and the levelling benchmarks. A comparison is

shown for points falling in urban and rural areas for both the ERS and ENVISAT data sets, the locations of which are marked of fig.6. The comparison further confirms earlier conclusions that the predominant source of error is in points displaying intermittent coherence (rural areas), as they are noisier than those displaying constant coherence (urban areas).

The noise in rural areas may be a combination of a number of factors, principally that the low number of interferograms ($m$) will increase the noise in the measurement simply by reducing the number of observations and decreasing the redundancy in the observations. However, land level in the rural sites may also be subject to environmental noise, such as soil shrink/swell, ploughing and tilling, the seasonal growth and harvest of crops and the loss of leaf cover for broadleaf trees during the winter period. The interaction of these effects with the radar signal is complex, depending also upon the geometry and moisture characteristics of plant and soil. Therefore, what we detect in a deformation signal using an ISBAS analysis is likely to be a combination of all of these factors and any underlying signal due to reservoir depletion or injection may be difficult to identify without filtering.

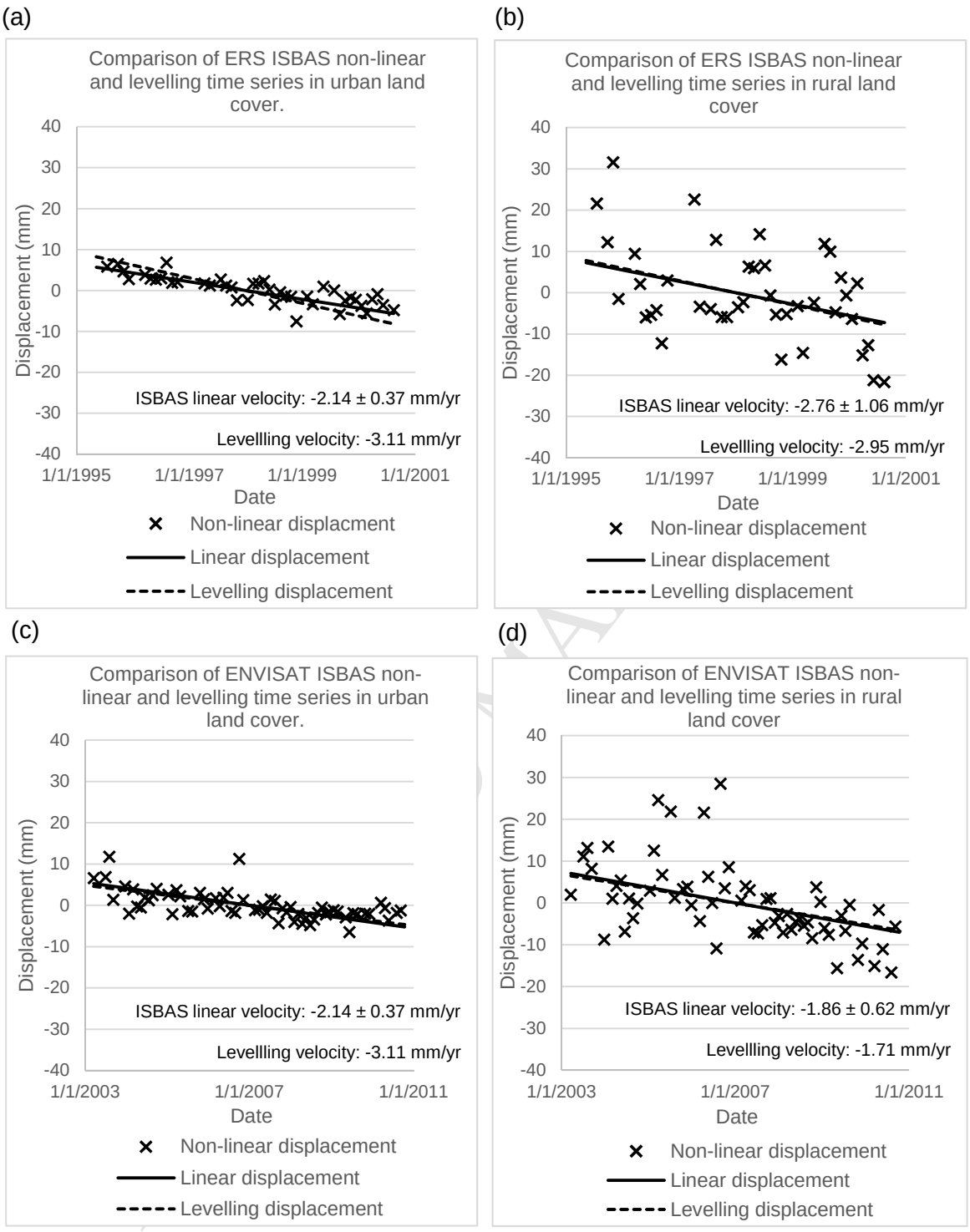


**Fig. 11.** Comparison of levelling benchmarks and neighbouring non-linear ISBAS analysis. The crosses represent non-linear ISBAS displacements, the solid linear trend

lines represent the linear ISBAS displacements and the dashed linear trend lines represent the linear levelling displacements. (a) ERS ISBAS in urban land cover (b) ERS ISBAS in rural land cover (c) ENVISAT ISBAS in urban land cover (d) ENVISAT ISBAS in rural land cover.

## 5. Comparisons with PSI Results from the TVP

The TVP compared unidentified PSI outputs from four OSPs and a result from TU Delft against levelling data for the Alkmaar site (Crosetto et al., 2008; Hanssen et al., 2008). These are compared with ISBAS results for the ERS and ENVISAT data sets (fig. 12).

It is useful to note here that the individual point results generated by the OSPs and TUD were not available to this analysis. Therefore, we are unable to comment upon the spatial resolution of the PSI results, which would have been almost an order of magnitude better than the ISBAS point measurements.

### *5.1 Comparison of Spatial Patterns and Coverage*

The PSI analysis identified the same spatial pattern of subsidence to the west of Alkmaar when compared with the ISBAS linear velocities (fig. 12). The comparison verifies that where PSI coverage has been possible, velocities are similar, significantly also identifying Alkmaar as being stable with subsidence to the west in the proximity of the Bergermeer reservoir. In agreement with the ISBAS results, the OSP's also found greater levels of subsidence in the ERS data than in the ENVISAT data. The PSI results are available from Hanssen et al. (2008, p.19-20).

The identification of subsidence to the west of Alkmaar is much clearer from the ISBAS point density (fig. 12a and fig.12b). This is due to the general observation that PSI only produces point velocities of a significant density over urban regions, which predominantly only show subsidence in the west of Alkmaar, and limited velocities over the Bergermeer reservoir in the town of Bergen. The inconsistent coverage of the PSI surveys has meant that a clear subsidence pattern may not be formed over the whole area (fig. 12c and fig. 12d).

It should be noted that the high quality ISBAS points, where coherence is constant (i.e. $m$=294 for ERS and $m$=636 for ENVISAT), fall mainly in the urban areas in approximately in the same locations as the OSP's PSI analyses (fig. 12e and fig.12f). This illustrates the capability of the ISBAS analysis to produce meaningful results in such areas, as well as the rural land classes. The benefit of relaxing the needs for coherence to be present in every interferogram is evident, with the ERS and ENVISAT ISBAS analysis covering a far greater portion of the scene. ISBAS is able to demonstrate that subsidence occurs across this region, something that the PSI results shown here were unable to achieve.

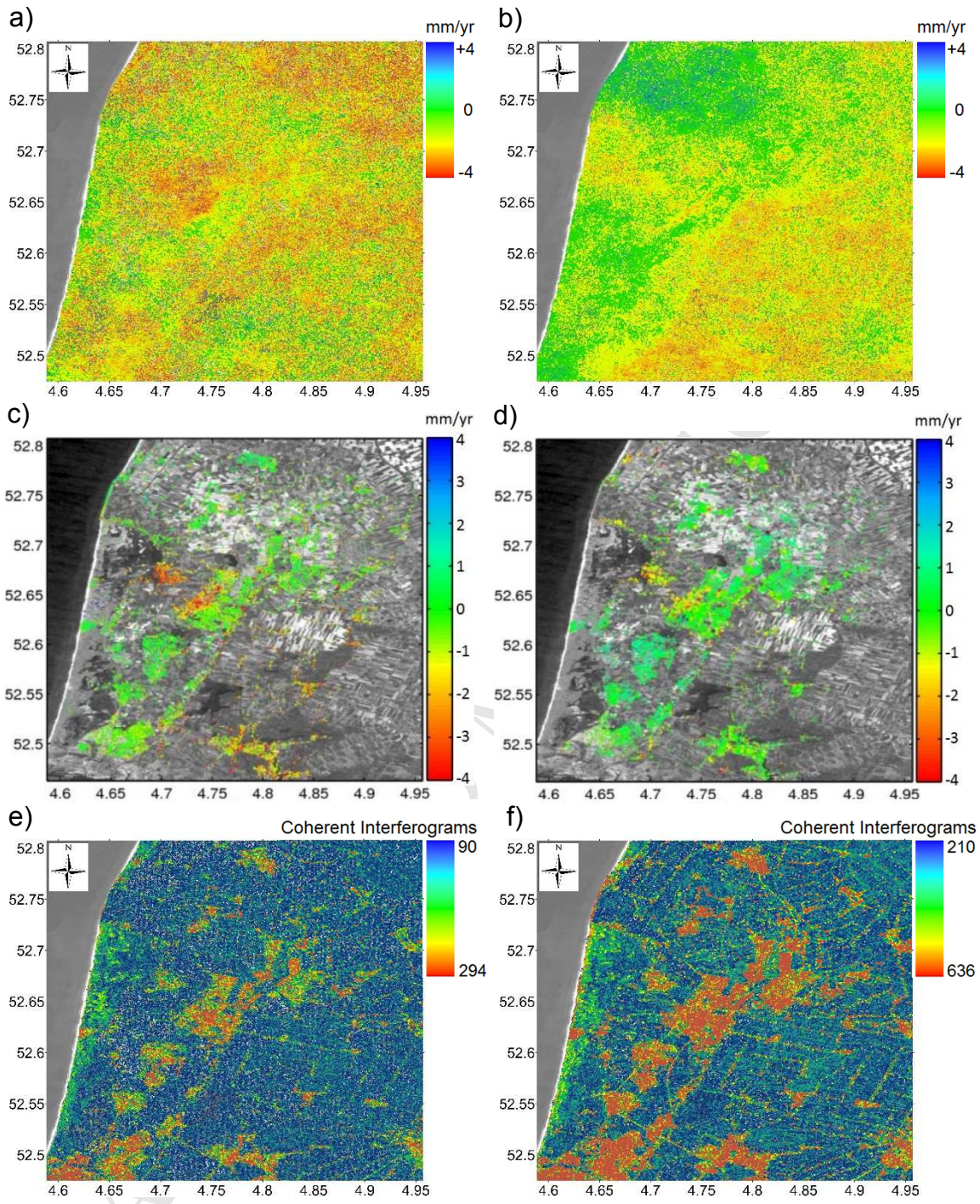


**Fig. 12.** (a) ERS ISBAS vertical velocities (b) ENVISAT ISBAS vertical velocities (c) ERS PSI from OSP D (from Hanssen et al., 2008) (d) ENVISAT PSI from OSP D (from Hanssen et al., 2008) (e) ERS ISBAS coherent interferograms per point (*m*) (f)

ENVISAT ISBAS coherent interferograms per point (*m*). The centre of Alkmaar is located at 52.63N 4.75E and the centre of Bergen is located at 52.67N 4.71E.

*5.2 Comparison of Linear Displacement Velocities*

The TVP concluded that the RMSE of the differences between PSI-levelling were between 1.04 – 1.54 mm/year for the ERS time series and 1.26 – 1.79 mm/year for ENVISAT (Table 5). These results are comparable with the RMSE of ISBAS-levelling shown in Table 5: 1.52 mm/year for the ERS time series and 1.13 mm/year for the ENVISAT time series. The ERS ISBAS analysis has produced a result which is within the error achieved using PSI; the ENVISAT ISBAS analysis proved more accurate than all five TVP results, with an RMSE 0.13mm/year smaller than the most accurate PSI result. ISBAS products have therefore produced similar accuracies to PSI with the significant benefit of an output that covered almost the complete scene.

| | ***ISBAS*** | ***TVP A*** | ***TVP B*** | ***TVP C*** | ***TVP D*** | ***TVP E*** |
|---|---|---|---|---|---|---|
| **ERS** | | | | | | |
| No. of Benchmarks | 128 | 36 | 151 | 58 | 58 | 47 |
| RMSE DInSAR-Levelling (mm/yr) | 1.52 | 1.07 | 1.54 | 1.04 | 1.23 | 1.18 |
| **ENVISAT** | | | | | | |
| No. of Benchmarks | 187 | 76 | 118 | 80 | 49 | 90 |
| RMSE DInSAR-Levelling (mm/yr) | 1.13 | 1.51 | 1.79 | 1.63 | 1.26 | 1.54 |

**Table 5**

A comparison of the RMSE ISBAS-levelling (mm/year) and the PSI-levelling (mm/year) from five products used in the TVP.

*5.3 Comparison of Non-Linear Displacements*

Unfortunately, non-linear displacements from the PSI results were only available for a single point (Hanssen et al., 2008) and there was no ISBAS coherent point within 50m of sufficient quality for a realistic comparison. We were therefore unable to complete this part of the analysis.

## 6. Discussion

The history of the Bergermeer gas reservoir confirms the ISBAS displacements in time and space. The deformation measured during the ERS observation period (1995-2000) corresponds with the exploitation of the reservoir until 2007 and consequent decline in pressure that resulted in subsurface compaction. The reservoir was converted into a gas storage site after 2007, where injection of cushion gas commenced to bring pressure to a workable operating value. The ENVISAT results (2003-2010) reflect these increasing pressure values in the Upper Rotliengend Group (Fokker et al., 2016). In space, differential ISBAS displacements over Bergermeer are characterized by higher subsidence in the northeastern sector, in agreement with the occurrence of two compartments separated by a narrow NW-SE trending fault (Orlic et al., 2013) which generated four earthquakes between 1994 and 2001.

Based upon the ISBAS displacements for the ERS time span (fig. 13a), the forward model of Mogi (1958) (fig. 13b) has been constructed to match surface subsidence with reservoir compaction within the Bergermeer reservoir, following the point pressure approach and considering a layered subsurface with non-uniform mechanical properties (Manconi et al., 2007). The model utilized a decreasing pore pressure of ≈10 MPa, as reported by the Netherlands Organization for Applied Scientific Research (TNO, 2008) for the corresponding time period, along with the elastic parameters for the different geological units (Young's modulus and Poisson ratio) available in Fokker et al. (2016). The nucleus of strain approach proposed by Geerstma, which more accurately simulates reservoir compaction due to production pressure depletion (Geertsma and Van Opstal, 1973), could not be formulated due to the lack of local pressure change data within the reservoir.

The best displacement pattern resembles five main sources of contraction with a radius ranging between 80m and 150m, located in the Upper Rotliengend Group, near the well trajectories, at depths of ~2100m. The overburden encompasses non-uniform elastic parameters with decreasing Young's modulus towards the surface, so the maximum vertical and radial displacements are amplified with respect to the homogeneous elastic model.

The estimated source parameters and the restricted uncertainties between the ISBAS LOS displacements and simulated deformation, are globally five times smaller than the ISBAS displacements (fig. 13b). The correspondence of ISBAS data, in turn, with NAP levelling data supports the quality our results.

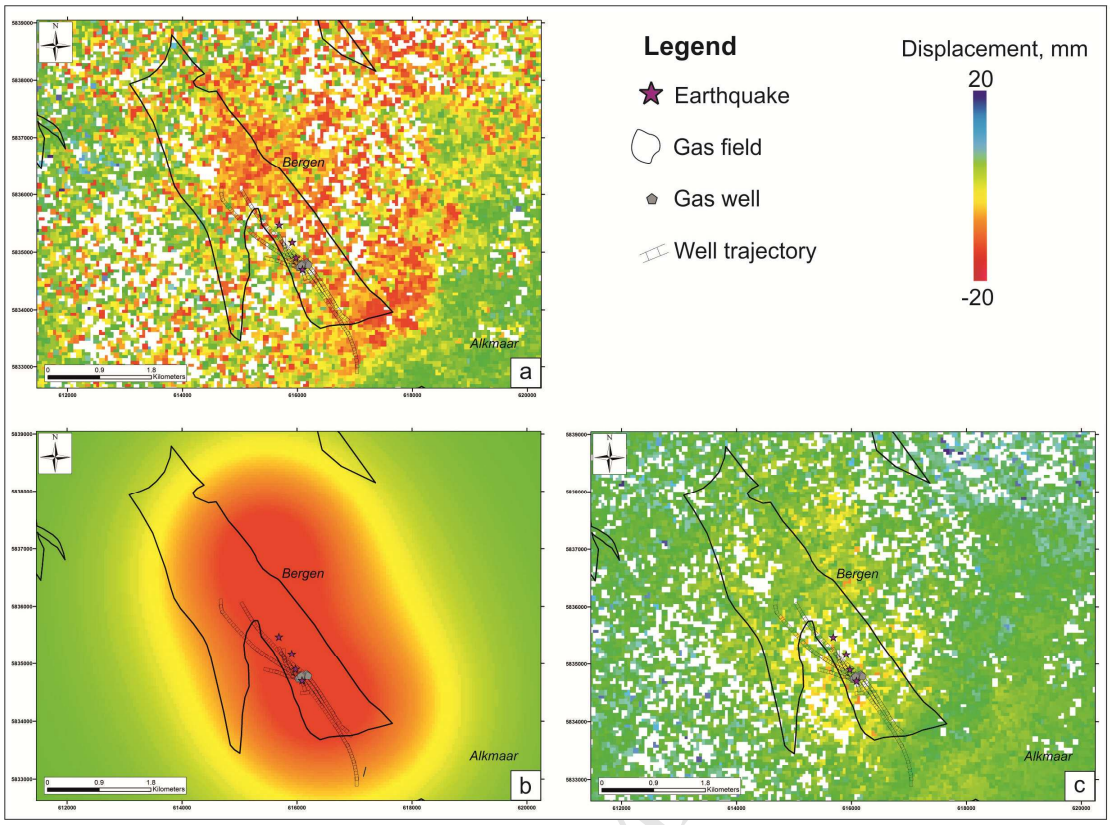


**Fig. 13.** (a) ISBAS LOS surface displacements at Bergermeer during 1995-2000. (b) Simulated LOS displacements determined by the Mogi model applied in this study. (c) Residual analysis shows that all layered models yield very good results in reproducing the observed surface displacement. Gas well and well trajectory data were attained from the Netherlands Oil and Gas Portal (http://www.nlog.nl/nl/home/NLOGPortal.html) and earthquake epicentre locations from the United States Geological Society earthquake archive (http://earthquake.usgs.gov/earthquakes/search/).

The advantages of the simplified semi-analytic elastic model adopted here are that only a few physical parameters have to be determined, producing a rudimentary calculation of the ground deformation patterns allowing for a more intuitive understanding of the

results. In addition, the model is relatively computationally inexpensive compared with the more accurate numerical solutions produced by Finite Element Methods (FEM), commonly adopted for simulating surface subsidence and reservoir compaction (e.g., Minkoff et al., 2003; Marketos et al., 2015). The effort required to adequately characterize complex constitutive models (e.g., material rheology, reservoir geometry, and inhomogeneity) and develop stable mesh attributes mean the repetitive calculations of complex simulations typical of FEM can make these approaches impractical.

The forward modelling proves that regular spatial sampling of DInSAR measurements are critical to better constrain the source parameters (Hanssen et al., 2008). In cases where a dense coverage is not possible, such as in vegetated areas, it may be necessary to supplement DInSAR measurements with ground survey observations, such as GNSS and levelling campaigns (Heimlich et al, 2015), or place a network of artificial scatterers, such as corner reflectors (Ferretti et al., 2007), in order to fill the gaps to complete the model.

The area between Bergen and Alkmaar is, indeed, vegetated and a clear gap of measurements is evident in each of the PSI results generated by the TVP. The ISBAS analysis suffers less from decorrelation in this area and regular sampling is preserved across the gap; therefore, we conclude that a more confident Mogi inversion may be applied using this data. Furthermore, with ISBAS it is not absolutely necessary to use additional ground surveys to return survey points in vegetated expanses.

## 7. Conclusions

This paper was undertaken to validate the ISBAS DInSAR method for the characterisation of land subsidence associated with oil and gas extraction and injection. When compared against levelling data, ISBAS velocities demonstrated an RMSE of 1.52 mm/year and 1.13 mm/year for the ERS and ENVISAT cases respectively, which compared very well to the PSI results obtained by the TVP (1.04 – 1.54 mm/year for ERS and 1.26 – 1.79 mm/year for ENVISAT). Non-linear displacements were in agreement with the trends set by the levelling in urban areas but greater noise was observed in the vegetated classes, which may be due to environmental factors (shrink/swell, canopy development, agricultural field preparation etc.) and contributions from the lack of coherence and redundancy in such areas. However, the main conclusion is that ISBAS products returned point velocities at almost every location in the scene, providing consistent coverage over the widest variety of land cover, including vegetated areas.

Finally, the improved point density and sampling of the ISBAS results implies a better input to any dislocation model to determine the approximate source location, depth and volume change responsible for the observed deflation at Bergerrmeer.

## Acknowledgements

The authors would like to acknowledge ESA for the provision of ERS and ENVISAT SAR data via the Category-1 project ID: 30113, the Rijkswaterstaat for the provision of precision levelling campaigns and Andrea Manconi for his valuable suggestions to improve the quality of the paper. Figures 12c-d were generated within the Terrafirma

Validation project, funded by the European Space Agency with ESRIN/Contract no 19366/05/I-EC (http://www.terrafirma.eu.com/product_validation.htm).

## References

Bateson, L., Cigna, F., Boon, D., Sowter, A., 2015. The application of the Intermittent SBAS (ISBAS) InSAR method to the South Wales Coalfield, UK. International Journal of Applied Earth Observation and Geoinformation, 34, pp.249-257.

Berardino, P., Fornaro, G., Lanari, R.,Sansosti, E., 2002. A new algorithm for surface deformation monitoring based on small baseline differential SAR interferograms. IEEE Transactions on Geoscience and Remote Sensing, 40(11), pp.2375-2383.

Bishop, C., Riddiford, F., Tourqu, A., Taylor, B, Hulm, E., 2004. Carbon dioxide storage in the In Salah Gas Project, Algerian Central Sahara, National Energy Technology Laboratory Library, Library http://www.netl.doe.gov/publications/proceedings/03/carbon-seq/pdfs/021.pdf (accessed April 2016)

Cigna, F., Rawlins, B. G., Jordan, C. J., Sowter, A., Evans, C. 2014. Intermittent Small Baseline Subset (ISBAS) InSAR of rural and vegetated terrain: a new method to monitor land motion applied to peatlands in Wales, UK. EGU General Assembly.

Crosetto, M., Monserrat, O. Agudo, M., 2008. Validation of existing processing chains in Terrafirma stage 2. Process Analysis Report, IG Inter-comparison, GMES TERRAFIRMA Project, ESRIN/Contract No. 19366/05/IE (Institute of Geomatica).

Crosetto, M., Monserrat, O., Iglesias, R., Crippa, B., 2010. Persistent Scatterer Interferometry. Photogrammetric Engineering & Remote Sensing, 76(9), pp.1061-1069.

Cuenca, M.C.,Hanssen, R., 2008. Subsidence due to peat decomposition in the Netherlands, kinematic observations from radar interferometry. In Proc. Fringe 2007 Workshop (pp. 1-6).

Davies R., Foulger, G., Bindley, A., Styles, P., 2013. Induced seismicity and hydraulic fracturing for the recovery of hydrocarbons. Marine and Petroleum Geology 45, 171-185. DOI:10.1016/j.marpetgeo.2013.03.016

Ferretti, A., 2014. Satellite InSAR Data: Reservoir Monitoring from Space, EAGE Publications BV, The Netherlands.

Ferretti, A., Fumagalli, A., Novali, F., Prati, C., Rocca, F., Rucci, A., 2011. A new algorithm for processing interferometric data-stacks: SqueeSAR. IEEE Transactions on Geoscience and Remote Sensing, 49 (9), 3460–3470.

Ferretti A., Prati C., Rocca F., 2001. Permanent Scatterers in SAR Interferometry. IEEE Transactions on Geoscience and Remote Sensing, v. 39 (I): 8-20.

Ferretti, A., Savio, G., Barzaghi, R., Borghi, A., Musazzi, S., Novali, F., Prati, C., Rocca, F., 2007. Submillimeter Accuracy of InSAR Time Series: Experimental Validation. IEEE Transactions on Geoscience and Remote Sensing, 45(5), doi: 10.1109/TGRS.2007.894440.

Fokker, P.A., Wassing, B.B.T., van Leijenb, F.J., Hanssen, R.F., Nieuwland, D.A., 2016. Application of an ensemble smoother with multiple data assimilation to the Bergermeer gas field, using PS-InSAR. Geomechanics for Energy and the Environment, 5, 16–28.

Galloway, D.L., Hudnut, K.W., Ingebritsen, S.E., Phillips, S.P., Peltzer, G., Rogez, F., Rosen, P.A., 1998. Detection of aquifer system compaction and land subsidence using interferometric synthetic aperture radar, Antelope Valley, Mojave Desert, California. Water Resources Research, 34(10), 2573–2585.

Geertsma, J., 1957. The effect of fluid pressure decline on volumetric changes of porous rocks: Transactions of the American Institute of Mining, Metallurgical and Petroleum Engineers, 210, 331.

Geertsma, J., 1966. Problems of rock mechanics in petroleum production engineering: Proceedings of the 1st International Society of Rock Mechanics Congress, 585–594.

Geertsma, J. and G. Van Opstal, 1973. A numerical technique for predicting subsidence above compacting reservoirs, based on the nucleus of strain concept: Verhandelingen Kon. Ned. Geol. Mijnbouwk, 28, 63–78.

Galloway, D.L., Hudnut, K.W., Ingebritsen, S.E., Phillips, S.P., Peltzer, G., Rogez, F., Rosen, P.A., 1998. Detection of aquifer system compaction and land subsidence using interferometric synthetic aperture radar, Antelope Valley, Mojave Desert, California. Water Resources Research, 34(10), 2573–2585.

Gluyas, J.G.,Cade, C.A., 1997. Sand compaction, American Association of Petroleum Geology memoir 69, 19-28.

Gong, W., Thiele, A., Hinz, S., Meyer, F.J., Hooper, A., Agram, P.S., 2016. Comparison of Small Baseline Interferometric SAR Processors for Estimating Ground Deformation. Remote Sens., 8, 330; doi:10.3390/rs8040330

Grötsch, J.,Gaupp, R., 2011. The Permian Rotliegend of the Netherlands. SEPM (Society for Sedimentary Geology).

Haak, H. W., Dost, B.,Goutbeek, F., 2001. Seismische analyse van de aardbevingen bij Alkmaar op 9 en 10 september en Bergen aan Zee op 10 oktober 2001. Koninklijk Nederlands Meteorologisch Instituut (in Dutch).

Hanssen, R. F., van Leijen, F.J., van Zwieten, G.J., Dortland, S., Bremmer, C.N.,Kleuskens M., 2008. Validation of PSI results of Alkmaar and Amsterdam within the Terrafirma validation project. Proc. of FRINGE 2007 Workshop, Frascati, Italy, 26 – 30 November 2007.

Heimlich, C., Gourmelen, N., Masson, F., Schmittbuhl, J., Kim, S.-W.,Azzola, J., 2015. Uplift around the geothermal power plant of Landau (Germany) as observed by InSAR monitoring. Geothermal Energy, 3:2, doi: 10.1186/s40517-014-0024-y.

Hole, J.K., Holley, R.J., Giunta, G., De Lorenzo, G., Thomas, A.M., 2012. InSAR assessment of pipeline stability using compact active transponders. Proc. ‘Fringe 2011 Workshop’, Frascati, Italy, 19–23 September 2011.

Hooper A., 2008. A multi-temporal InSAR method incorporating both persistent scatterer and small baseline approaches. Geophysical Research Letters, v.35, L16302, doi:10.1029/2008GL034654.

Hooper, A., Bekaert, D., Spaans, K., Arikan, M., 2012. Recent advances in SAR interferometry time series analysis for measuring crustal deformation. Tectonophysics, 514-517, 1-13, doi: 10.1016/j.tecto.2011.10.013.

Hooper, A., Zebker, H., Segall, P., Kampes, B., 2004. A new method for measuring deformation on volcanoes and other natural terrains using InSAR persistent scatterers. Geophys. Res. Lett., 31 (23), L23611. DOI: 10.1029/2004GL021737

Kaasschieter, J.P.H. and Reijers, T.J.A. (1982). Petroleum Geology of the Southeastern North Sea and the Adjacent Onshore Areas. Vol. 62, No. 1, Springer Science & Business Media, The Hague, Netherlands.

Kampes, B., 2005. Displacement Parameter Estimation using Permanent Scatterer Interferometry, Ph.D. Thesis, Technische Universiteit Delft.

Kooi, H., de Vries, J.J., 1998. Land subsidence and hydrodynamic compaction of sedimentary basins. Hydrol. Earth Syst. Sci. 2, 159-171, 1998. DOI:10.5194/hess-2-159-1998

Lanari, R., Casu, F., Manzo, M., Zeni, G., Berardino, P., Manunta, M., Pepe, A., 2007. An overview of the small baseline subset algorithm: A DInSAR technique for surface deformation analysis, Pure Appl. Geophys., 164, 637–661, doi:10.1007/s00024-007-0192-9.

Leifer, I., Lehr, W.H., Simecek-Beatty, D., Bradley, E., Clark, R., Dennison, P., Hu, Y., Matheson, S., Jones, C.E., Holt, B., Reif, M., Roberts, D.A., Svejkovsky, J., Swayze, G., Wozencraft, J., 2012. State of the art satellite and airborne marine oil spill remote

sensing: Application to the BP Deepwater Horizon oil spill. Remote Sensing of the Environment 124, 185–209. DOI:10.1016/j.rse.2012.03.024

Li, T., Liu, G., Lin, H., Jia, H., Zhang, R., Yu, B., Luo, Q., 2014. A Hierarchical Multi-Temporal InSAR Method for Increasing the Spatial Density of Deformation Measurements. Remote Sens., 6, 3349-3368; doi:10.3390/rs6043349.

Lorenz, G.K., van Beusekom, W., Groenewoud W., Hofman, M., 1995. Geodetic determination of land subsidence in the Netherlands. In: Barends, F.B.J., Brouwer, F.J.J., Schoder, F.H. (Eds.), Land Subsidence. IAHS Publ. 234, 187-196.

Manconi, A., Walter, T.R., Amelung, F., 2007. Effects of mechanical layering on volcano deformation. Geophys. J. Int., 170(2), 952-958.

Marinkovic, P., Ketelaar, G., van Leijen, F. and Hanssen, R., 2007. InSAR quality control: Analysis of five years of corner reflector time series. In Proceedings of Fringe 2007 Workshop (ESA SP-649), Frascati, Italy (pp. 26-30).

Marketos, G., Govers, R., Spiers, C.J., 2015. Ground motions induced by a producing hydrocarbon reservoir that is overlain by a viscoelastic rocksalt layer: a numerical model. Geophys. J. Int., 203, 228-242, 10.1093/gji/ggv294.

Mathieson, A., Wright, I. Roberts, D. M.,Ringrose, P. S., 2009. Satellite Imaging to Monitor CO2 Movement at Krechba, Algeria. Energy Procedia, 1(1), February 2009, 2201-2209.

Minkoff, S.,E., Stone, C.M., Bryant, S., Peszynska, M., Wheeler, M.F., 2003. Coupled fluid flow and geomechanical deformation modeling. Journal of Petroleum Science and Engineering, 38, 37- 56, doi:10.1016/S0920-4105(03)00021-4

Mogi, K., 1958. Relations between the eruptions of various volcanoes and the deformations of the ground surface around them. Bull. Earth. Res. Inst., University of Tokyo, 36, pp.99–134.

Mora O., Mallorquí J.J., Broquetas A., 2003. Linear and nonlinear terrain deformation maps from a reduced set of interferometric SAR images. IEEE Transactions on Geoscience and Remote Sensing, v. 41: 2243-2253.

Nagel, N., 2001. Compaction and subsidence issues within the petroleum industry: From Wilmington to Ekofisk and beyond. Physics and Chemistry of the Earth, Part A: Solid Earth and Geodesy, 26, pp.3-14.

Novellino, A., Athab, A. D., Bin Che Amat, M. A., Syafiudin, M. F., Sowter, A., Marsh, S., Cigna, F.,Bateson, L., 2014a. Intermittent SBAS Ground Motion Analysis in Low Seismicity Areas: Case Studies in the Lancashire and Staffordshire coal-fields, UK. Seismology from Space: Geodetic Observations and Early Warning of Earthquakes. Royal Astronomical Society, Burlington House, Piccadilly, London, UK.

Novellino, A., Cigna, F., Jordan, C., Sowter, A., Calcaterra, D., 2014b. Monitoring large-scale landslides and their induced hazard with COSMO-SkyMed Intermittent SBAS (ISBAS): a case study in north-western Sicily, Italy. In EGU General Assembly Conference Abstracts (Vol. 16, p.9621).

Onumaa, T., Ohkawa, S., 2009. Detection of surface deformation related with CO2 injection by DInSAR at In Salah, Algeria. Energy Procedia, 1, 2177-2184.

Orlic, B., Wassing, B.B.T., Geel, C.R., 2013. Field scale geomechanical modeling for prediction of fault stability during underground gas storage operations in a depleted gas

field in the Netherlands. In 47th US Rock Mechanics / Geomechanics Symposium held in San Francisco, CA, USA, 23-26 June 2013 Alexandria, VA: ARMA, American Rock Mechanics Association.

Osmanoğlu, B., Sunar, F., Wdowinski, S.,Cabral-Cano, E., 2015. Time series analysis of InSAR data: Methods and trends. ISPRS Journal of Photogrammetry and Remote Sensing.

Pepe, A., Berardino, P., Bonano, M., Euillades, L.D., Lanari, R., Sansosti, E., 2011. SBAS-Based Satellite Orbit Correction for the Generation of DInSAR Time-Series: Application to RADARSAT-1 Data, IEEE Transactions on Geoscience and Remote Sensing, 49(12), 5150-5165, doi: 10.1109/TGRS.2011.2155069

Pepe, A., Sansosti, E., Berardino, P., Lanari, R., 2005. On the Generation of ERS/ENVISAT DInSAR Time-series via the SBAS Technique, IEEE Geosci. Remote Sens. Lett., 2, 265–269, doi:10.1109/LGRS.2005.848497

Ringrose, P., Atbi, M., Mason, D., Espinassous, M., Myhrer, Ø., Iding, M., Mathieson, A., Wright, I.,2009. Plume development around well KB-502 at the In Salah CO2 storage site. First Break, 27(1), pp.85-89.

Schmidt, D. A., Bürgmann, R., 2003. Time-dependent land uplift and subsidence in the Santa Clara valley, California, from a large interferometric synthetic aperture radar data set, J. Geophys. Res., 108(B9), 2416, doi:10.1029/2002JB002267.

Sowter, A., Bateson, L., Strange, P., Ambrose, K. and Fifik Syafiudin, M.F., 2013. DInSAR estimation of land motion using intermittent coherence with application to the

South Derbyshire and Leicestershire coalfields. Remote Sensing Letters, 4(10), pp.979-987.

Sowter, A., Amat, M.B.C., Cigna, F., Marsh, S., Athab, A. and Alshammari, L., 2016. Mexico City land subsidence in 2014–2015 with Sentinel-1 IW TOPS: Results using the Intermittent SBAS (ISBAS) technique. International Journal of Applied Earth Observation and Geoinformation, 52, pp.230-242.

Suckale, J., 2009. Induced seismicity in hydrocarbon fields. Advances in geophysics, 51, pp.55-106.

Terzaghi, K., 1925. Principles of soil mechanics, IV, Settlement and consolidation of clay, Eng. News Rec., 95(3), 874–878.

TNO, 2008. Netherlands Organization for Applied Scientific Research. TNO 2008-U-R1071/B.

TNO, 2015. Recent developments on the seismicity of the Groningen field in 2015. TNO 2015 R10755

Van Adrichem Boogaert, H.A.,1976. Outline of the Rotliegend (Lower Permian) in the Netherlands. In The Continental Permain in Central, West, and South Europe (pp. 23-37). Springer Netherlands.

Van Eck, T., Goutbeek, F., Haak, H., Dost, B., 2006. Seismic hazard due to small-magnitude, shallow-source, induced earthquakes in The Netherlands. Engineering Geology, 87, 105–121, doi:10.1016/j.enggeo.2006.06.005

Van Eijs, R.M.H.E., Mulders, F.M.M., Nepveu, M., Kenter, C.J., Scheffers, B.C., 2006. Correlation between hydrocarbon reservoir properties and induced seismicity in the Netherlands. Engineering Geology, 84, 99-111, doi:10.1016/j.enggeo.2006.01.002

Van Gent, H., Urai, J.L.,De Keijzer, M.,2011. The internal geometry of salt structures–A first look using 3D seismic data from the Zechstein of the Netherlands. Journal of Structural Geology, 33(3), pp.292-311.

Van Lith, J.G.J.,1983. Gas Fields of Bergen Concession, The Netherlands. Petroleum Geology of the Southeastern North Sea and the Adjacent Onshore Areas. Springer.

Van Thienen-Visser, K.,Breunese, N., (2015). Induced seismicity of the Groningen gas field: History and recent developments. The Leading Edge 34 (6), 664-671. DOI: 10.1190/tle34060664.1

Van Wees J.D., Buijze, L., VanThienen-Visser, K., Nepveu, M., Wassing, B.B.T., 2014. Geothermics, 52, 206–219, doi: 10.1016/j.geothermics.2014.05.004

Wilson, M.P., Davies, R.J., Foulger, G.R., Julian, B.R., Styles, P., Gluyas, J.G., Almond S., 2015. Anthropogenic earthquakes in the UK: A national baseline prior to shale exploitation. Marine and Petroleum Geology 67, 1-17, doi:10.1016/j.marpetgeo.2015.08.023

Yang, Q., Zhao, W., Dixon, T.H., Amelung, F., Han, W.S., Li, P., 2015. InSAR monitoring of ground deformation due to CO2 injection at an enhanced oil recovery site, West Texas. International Journal of Greenhouse Gas Control, 41, 20–28, doi: 10.1016/j.ijggc.2015.06.016

Zoback, M.D., Zinke, J.C., 2002. Production-induced normal faulting in the Valhall and Ekofisk oil fields. Pure Appl. Geophys. 159, 403-420.

## Appendices

| *Sensor* | *Date* | $B_{\perp}$ *(m)* | *Date* | $B_{\perp}$ *(m)* |
|---|---|---|---|---|
| ERS-2 SAR | 27th August 1997 | 0 | 29th April 1998 | -54 |
| | 19th July 1995 | -424 | 3rd June 1998 | 95 |
| | 27th September 1995 | -137 | 8th July 1998 | -1015 |
| | 1st November 1995 | 248 | 12th August 1998 | -460 |
| | 6th December 1995 | -566 | 16th September 1998 | -867 |
| | 20th March 1996 | -51 | 21st October 1998 | -722 |
| | 24th April 1996 | 97 | 25th November 1998 | -975 |
| | 29th May 1996 | -706 | 3rd February 1999 | -536 |
| | 3rd July 1996 | -158 | 10th March 1999 | -793 |
| | 7th August 1996 | -235 | 19th May 1999 | -330 |
| | 11th September 1996 | -709 | 28th July 1999 | 79 |
| | 16th October 1996 | -151 | 1st September 1999 | -1013 |
| | 20th November 1996 | 653 | 6th October 1999 | -660 |
| | 9th April 1997 | 174 | 10th November 1999 | -158 |
| | 14th May 1997 | -483 | 15th December 1999 | -282 |
| | 23rd July 1997 | -359 | 19th January 2000 | -637 |
| | 1st October 1997 | -401 | 23rd February 2000 | -1170 |
| | 5th November 1997 | -986 | 29th March 2000 | -437 |
| | 14th January 1998 | -626 | 3rd May 2000 | -477 |
| | 18th February 1998 | -381 | 7th June 2000 | -774 |
| | 25th March 1998 | -447 | 16th August 2000 | -540 |

**Table A.1**

ERS-2 SAR image dates and perpendicular baselines $B_{\perp}$ (m) in reference to the master image on 27th August 1997.

| *Sensor* | *Date* | $B_{\perp}$ *(m)* | *Date* | $B_{\perp}$ *(m)* |
|---|---|---|---|---|
| ENVISAT ASAR | 11th July 2007 | 0 | 28th March 2007 | 591 |
| | 19th March 2003 | 117 | 2nd May 2007 | -103 |
| | 2nd July 2003 | -343 | 6th June 2007 | 57 |
| | 6th August 2003 | -392 | 15th August 2007 | 87 |
| | 10th September 2003 | 290 | 19th September 2007 | 597 |
| | 24th December 2003 | 300 | 24th October 2007 | -126 |
| | 28th January 2004 | 681 | 28th November 2007 | 367 |
| | 3rd March 2004 | -179 | 2nd January 2008 | -319 |
| | 7th April 2004 | 834 | 6th February 2008 | 317 |
| | 12th May 2004 | -415 | 12th March 2008 | 27 |
| | 16th June 2004 | 74 | 16th April 2008 | 389 |
| | 21st July 2004 | 283 | 21st May 2008 | 35 |
| | 25th August 2004 | 146 | 25th June 2008 | 230 |
| | 29th September 2004 | -517 | 30th July 2008 | 134 |
| | 12th January 2005 | -519 | 3rd September 2008 | 398 |
| | 16th February 2005 | -321 | 8th October 2008 | 28 |
| | 23rd March 2005 | -717 | 12th November 2008 | 191 |
| | 27th April 2005 | 451 | 17th December 2008 | -140 |
| | 6th July 2005 | 642 | 21st January 2009 | 258 |
| | 10th August 2005 | -66 | 25th February 2009 | 184 |
| | 19th October 2005 | 149 | 6th May 2009 | -108 |
| | 23rd November 2005 | 336 | 10th June 2009 | 260 |
| | 28th December 2005 | 363 | 15th July 2009 | 191 |
| | 8th March 2006 | 203 | 19th August 2009 | 68 |
| | 12th April 2006 | -425 | 28th October 2009 | 36 |
| | 17th May 2006 | -79 | 2nd December 2009 | 198 |
| | 21st June 2006 | 176 | 17th March 2010 | 146 |
| | 26th July 2006 | 704 | 21st April 2010 | 456 |
| | 30th August 2006 | 647 | 26th May 2010 | 14 |
| | 4th October 2006 | -647 | 4th August 2010 | -175 |
| | 8th November 2006 | -388 | 8th September 2010 | 139 |
| | 21st February 2007 | 171 | | |

**Table A.2**

ENVISAT ASAR image dates and perpendicular baselines $B_{\perp}$ (m) in reference to the master images on 11$^{th}$ July 2007.

The ISBAS method can detect land motion over gas fields for all land cover types.
The density of measurements was uniform over almost the entire land surface.
The coverage appears significant when compared to PSI surveys of the same area..
The accuracy is better than 1.52 mm/year when compared to ground levelling data.
The ISBAS method improves the capability to infer the properties of buried cavities.